The Horní Benešov ore deposit in the Devonian Šternberk-Horní Benešov Belt, Jeseníky Mts, Czech Republic. Part II: Fe-ore occurrences

Arno Mücke, Zdeněk Dolníček, Bohuslav Fojt, Jana Hladíková,
Marta Pudilová, Jaroslav Reif & Radek Škoda

Abstract: The iron ore mineralizations at the Horní Benešov sulphidic deposit are located in the Devonian Šternberk-Horní Benešov Belt which is enveloped by the Lower Carboniferous flysch of the Culm Foreland Basin. The belt consists of metasedimentary and metavolcanic rocks. Horní Benešov is the only site in the Jeseníky Mountains, where the oxidic iron ores occur in close association with the sulphide orebodies of the VMS/SHMS type.

The ores are composed of magnetite, Fe-silicates [stilpnomelane, often Ba-dominated, chamosite, berthierine and odinite (in the former literature described as greenalite)], carbonates (calcite, siderite, rhodochrosite and rarely dolomite and ankerite), sulphides (pyrite, sphalerite, galena, arsenopyrite, chalcopyrite, cobaltite and a mineral of the linneite-group with unusual composition), apatite, krauskopfite, barite and scheelite. Fluid inclusion and stable isotope data are in agreement with a low-temperature metamorphic/diagenetic reworking of the ores, which does not exceed 200-250 °C. These low temperatures are also confirmed by the abundance of clastic material and fossils which both survived metamorphism, occurrence of stilpnomelane, diffusively zoned Fe-Mn carbonate crystals and remnants of undigested material in replacement textures. The associated fluids were low-salinity (1-5 wt. % NaCl eq.), high-δ^{18}O (+8 to +19 ‰ SMOW) aqueous solutions belonging to the Na-Mg-Cl salt system. The post-metamorphic fluid evolution involved the zero-salinity meteoric waters (with negative δ^{18}O values) and high-salinity Ca-Na-Cl brines. The isotope data suggest participation of sulphur derived from the reduction of marine sulphate and carbon from organic matter during the formation of pyrite and carbonate, respectively. However, the latter originated predominantly from CO_2-rich volcanogenic exhalations.

The studied iron mineralizations are characterized by the absence of ooids, low abundance of hematite, presence of Mn/Fe carbonates and the absence of basic volcanites in the immediate contact with iron ores. The iron ores differ from the typical Lahn-Dill type and therefore, they may represent the iron-rich distal facies of hydrothermal vents which gave rise to the polymetallic sulphide + barite deposit at Horní Benešov. However, magnetite was formed by the replacement of primary siderite or is inferred to originate, at least partially, from precipitation of Fe-rich fluids.

Key words: Šternberk – Horní Benešov Belt, iron mineralization, mineralogy (carbonates and Fe-silicates), fluid inclusions, stable isotopes, mineral-, whole rock- and REE-chemistry, genesis

Introduction

In the Devonian Šternberk-Horní Benešov Belt, close to the eastern border of the Rhenohercynian Zone (Franke & Żelaźniewicz 2000), a few of small iron bearing occurrences are located. In former time, some of these occurrences were mined. In the relevant German literature (published in the beginning of the 20th century) the localities are known as Tillersberg (Vršina) and Steinhübel. All these occurrences are located in the wide vicinity of the sulphide deposit of Horní Benešov.

When mining of the iron ore within the Horní Benešov area reached the highest activity during the 19th century, the iron ores were completely used for the Vítkovice (Ostrava) Iron Company (Kruťa 1958). Exploration activities during the World War II led to the recognition of about 500 000 tons of iron ore occurring up to a depth of 200 m (Zelinger 1998). Some iron occurrences were discovered also after the mapping by Janečka & Skácel (1950) with the help of drilling activities (Kučera 1957).

In the course of renewed exploration and mining activities within the area of the Zn-Pb deposit at Horní Benešov taking place in the years between 1950 and 1992, a variety of small iron-bearing lenses were found. These lenses occur close to the sulphide-bearing bodies of the western part of the Devonian volcano-sedimentary complex. This paper is focused on these iron mineralizations only, whereas the sulphide deposits of Horní Benešov were recently described by Fojt et al. (2010).

Iron ores from Horní Benešov in the literature

A first detailed report about the iron ore was published by Kretschmer (1917). According to this author, the occurrence at Steinhübel was of high economic importance because the ore body had a length of 50 to 95 m and a thickness of more than 2 m (sometimes up to 14 m). The mafic host rocks were characterized as "Spilitmandelstein" and along the hanging wall as "Schalstein". According to Kretschmer (1918) the ore mineralization consisted of magnetite, thuringite (= chamosite), stilpnomelane, jaspilite (= ferruginuous quartz), viridite (= a Fe-alumosilicate), moravite (= a type of chlorite), and mackensite (= a hydrous ferric alumosilicate) of which the underlined minerals are discredited today.

Based on 13 drill cores (down to a depth of 180 m) carried out in the area south of Horní Benešov, Karrenberg-Metz & Quitzow (1942) described an iron-ore zone of 2 to 2.5 km in length. The same authors stated that the mineralized zone is associated with isoclinal folded "Schalstein" and carbonate belonging to the lower part of the middle Devonian, obviously in a reverse tectonic setting. In a normal tectonic setting, however, the authors observed the following rocks: in the hanging wall a calcareous iron ore (= kalkiges Erz) and in the lying foot wall an acidic Fe ore (= kieseliges Roteisenerz). The latter has a thickness of about

1.5 m, locally 6 m and in exception up to 10 m. Average Fe-content is 24 % in the calcareous ore and 31 % in the acidic ore. Similar to Kretschmer (1917, 1918), Karrenberg-Metz & Quitzow (1942) correlated the iron content with the presence of either magnetite and hematite or iron-silicates. Characteristic textural features of the ores are described by the aforementioned authors including ooids, relics of fossils, sometimes irregularly layered mixtures of hematite + quartz, magnetite and other minerals. Relics of jelly-like textures often showing shrinkage cracks caused by dehydration were also mentioned. The authors supposed a genesis identical to the well-known Lahn-Dill type the origin of which is associated with basic volcanism and syngenetic sedimentation in a shallow-marine basin. Blastic fabrics originated either during superimposed diagenesis or Variscan regional metamorphism (Karrenberg-Metz & Quitzow, 1942).

The differentiation of the iron ores into the two types, calcareous and acidic, was later confirmed by Koutek (1951), Skácel (1959, 1960, 1966) and various other authors. Skácel (1960) observed varying quantities of iron ores. Similar to Karrenberg-Metz & Quitzow (1942), Skácel (1960) correlated the origin of iron ores with submarine volcanic exhalations associated with basic volcanism and stated that the acidic type of the middle-Devonian mineralization is located in a lower stratigraphic position than the calcareous type (Skácel 1959). Classifying the ore deposit, Skácel (1963b) used the former GDR terminology differentiating between the so-called "Grenzlagerstätte" (occurring in the hanging wall of the Upper Devonian sediments) and the iron ores which are completely enclosed in partly metamorphosed mixtures of volcanogenic material and sediments of Devonian age.

On the basis of rock textures, Skácel (1959, 1962) differentiated 12 ore types. In the area around Horní Benešov, he observed the so-called jaspilite ore, massive and layered hematite, magnetite and hematite enrichments, ore consisting of magnetite and Fe-chlorite (= chamosite), ore consisting of Fe-chlorite (= chamosite) associated with magnetite + siderite, limestones and tuffite both mineralized with finely dispersed hematite. Additionally Skácel (1963a, 1964, 1966) observed two further ore types, the brecciated and the fragmented ore. Another paper of Skácel (1965) deals with an ooidal ore type which seems to be relatively frequent in the Horní Benešov area especially in the deposit at "Steinhübel". Skácel (1960, 1965) supposed that the Horní Benešov iron mineralizations were formed in greater depth within the Devonian marine basin where exhalations occur. These exhalations were accompanied with submarine explosions causing water turbulences and thus the formation of ooids.

According to Chlupáč (1965), Dvořák et al. (1984) and Hladil et al. (1987), the Devonian Horní Benešov iron ores belonging to the Eifelian occur in calcareous schists and are completely enclosed in mafic volcanogenic rocks. However, Urbánek (1988) inferred that the oldest rocks of Devonian are of Frasnian age. On the other hand, according to the same authors, the iron ores are mostly concentrated along the contact between Upper Devonian hyaloclastite and limestone.

Rock types associated with iron ores are mentioned in the older literature, e. g. by Karrenberg-Metz & Quitzow (1942) as "Schalstein", spilite, limestone and calcareous schist. In a geological map which included the iron deposits "Tillersberg" and "Steinhübel" Janečka & Skácel (1950) mentioned the following rocks: diabase, amygdaloidal rocks, diabase tuffite and diabase porphyrite. These middle Devonian rocks are considered by

Janečka & Skácel (1950) and Kučera (1957) to be the source rocks. From a petrographic point of view the work by Barth (1960) is much more detailed, describing following rocks associated with iron ores: amygdaloidal and spilitic porphyrite and mixtures of them, spilite, lapilli tuffs, tuffitic ashes, tuffites, and sedimentary rocks containing admixtures of calcareous spilite and components of volcanogenic origin. Přichystal (1983, 1990) considered calcareous spilite and characterized it as peperite and hyaloclastite and described the occurrence of lithoclastic lapilli tuffs and tuffites.

Up to the 60's of the 20th century a suite of minerals was detected in the Horní Benešov area by Kretschmer (1917, 1918), Karrenberg-Metz & Quitzow (1942), Kruťa (1958) and Skácel (1959, 1960, 1962, 1964, 1965, 1966), including hematite, magnetite, pyrolusite, quartz, calcite, siderite, stilpnomelane, thuringite (= chamosite), pyrite and limonite. The list of minerals was enlarged in the years between 1985 and 2010 (Reif 1985, 1999, 2000a, 2000b, Reif & Vávra 2000, Houzar et al. 2010) by sphalerite, galena, chalcopyrite, pyrrhotite, arsenopyrite, rhodochrosite, scheelite, krauskopfite and tourmaline (=dravite).

The mineral composition of iron ores in the Šternberk-Horní Benešov Belt and some deposits of the Vrbno Group were characterized in the master's thesis of Kopecká (2012).
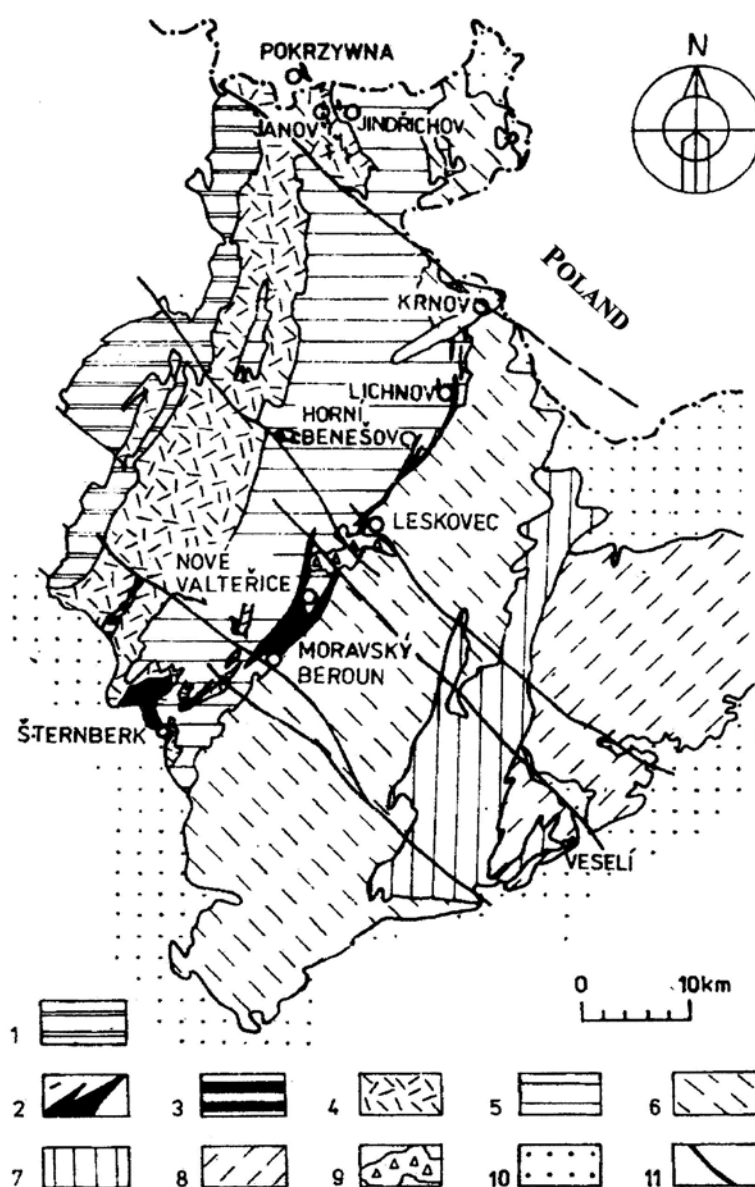

Fig 1: Schematic map of the wider neighbourhood of the Horní Benešov ore deposit (after Přichystal 1990). 1-Vrbno Group; 2-Šternberk-Horní Benešov Belt ; 3-Sovinec Devonian; 4-Andělská Hora Formation; 5-Horní Benešov Formation; 6-Moravice Formation, lower part; 7-Moravice Formation, upper part; 8-Hradec-Kyjovice Formation; 9-neovolcanites; 10-Tertiary, Quaternary and Cretaceous sediments; and 11-tectonic zones.

Short summary of the Geology of the Šternberk-Horní Benešov Belt

The Devonian Šternberk-Horní Benešov Belt located along the eastern border of the Bohemian Massif has a length of 42 km and a width varying between 0.2 and 2.5 km (Fig. 1). The first geological report on the belt was published by Roemer (1870) and later by Kretschmer (1917). Geological mapping by Janečka & Skácel (1950) and Kettner (1952) signifies this belt as "an island occurring within an anticline of the folded Culmian greywacke". Urbánek (1988) showed that three tectonic slices of Devonian rocks are present (i.e., Western, Central, and Eastern Devonian Zone) ranging in age from Eifelian via Givetian up to Frasnian. In the course of the Frasnian, the sedimentation of limestone and pelitic rocks occurred whereas during Tournaisian up to Viséan, the Devonian "islands" were enveloped by orogenic sediments (= flysch) (Fig. 2). During the Variscan orogeny, the rocks of the Horní Benešov area were deformed by dextral movement (Synek et al. 1990) followed by three folding events (Orel 1975).

Macro-analytical investigations on kinematics of deformations along the north-eastern border of the Bohemian Massif led Grygar & Vavro (1995) to the assumption that the area shows evidences of oblique collision occurring between the inner part of the Variscan zone and the terrain of the Brunovistulicum (Schulmann & Geyer 2000). According to Sawkins & Burke (1980) and Jakeš & Patočka (1982), the geotectonic position agrees with the island-arc setting, whereas Přichystal (1983, 1984) and Kalvoda et al. (2008) postulated the initial rift stage during which new ocean crust generated.

The index of crystallinity of the organic matter of the Devonian rocks ranges from 0.1 to 0.2 (Kříbek 1977) and the reflectivity of the organic material is characterized by R_{max} = 5.7 % and R_{min} = 1.4 – 3.8 % (Müller 1981). Deduced from both, the temperature of metamorphism of the investigated area lies between 200 and 250 °C.
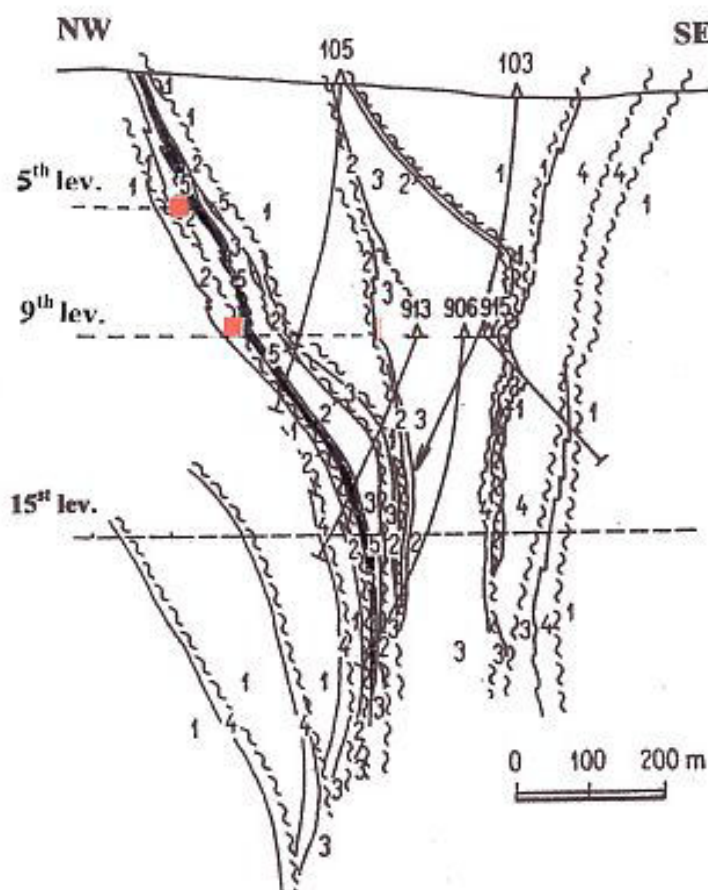

Fig 2: Schematic cross-section of the ore field after Urbánek (1988). 1-Carboniferous flysch sediments; 2-limestones, shales, breccias, interpositions of the volcanic rocks; 3-hyaloclastics, basaltic tuffs; 4-schists with Radiolaria; 5-breccias with sulphidic ore mineralization; waves -strata-dependent tectonic lines; red quadrangle - studied Fe-ore mineralizations.

Geological setting of the studied iron ores

The position of the occurrences of the iron ores at the polymetallic barite-bearing sulphidic Fe-Zn-Pb deposit is illustrated in Fig. 2. The description of the field situation given below is taken from Reif (2000a). Three objects have been sampled and investigated in a greater detail.

Object 1: Main rock type of the area, hosted by the Western Devonian Zone, are sericite schists (metatuffs and metatuffites). An irregularly shaped iron-ore lens (thickness 2 m) is located below the 5th level; mining block No. 612 (Fig. 3). From the mine documentation made by Kuba & Urbánek (1978) it is suggested that the iron ores form an elongated discontinuous lenticular body between the 4th and 7th mine level. The studied lens occurs in the underlying bed of the Devonian rocks and is enveloped by limestone and calcareous schist in a reverse tectonic setting. The hanging wall (of the iron lens), consisting of silicified calcareous schist, contains disseminated Fe, Zn, and Pb sulphides. The iron ore is associated with massive pyrite, accessory sphalerite and galena and locally stilpnomelane and calcite. Samples from object 1 have the label "BL".
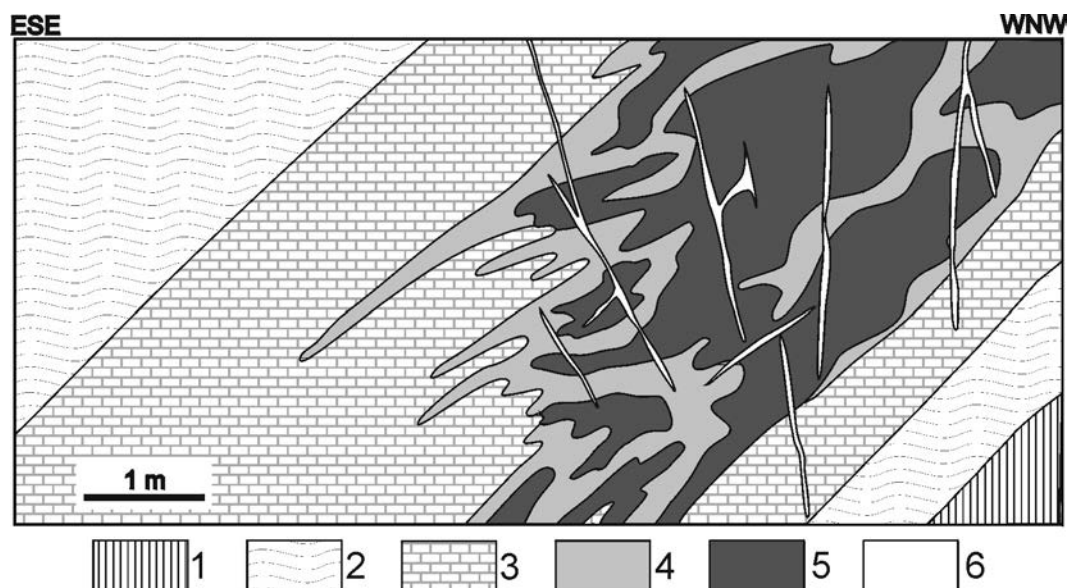
Fig 3: Schematic profile through the Fe-mineralization in mine block 612 according to mine documentation by Kuba and Urbánek (1978). 1-greywackes; 2-chlorite-sericite schists; 3-silicified limestones; 4-pyrite accumulations; 5-Fe ores; and 6-quartz-calcite veins.
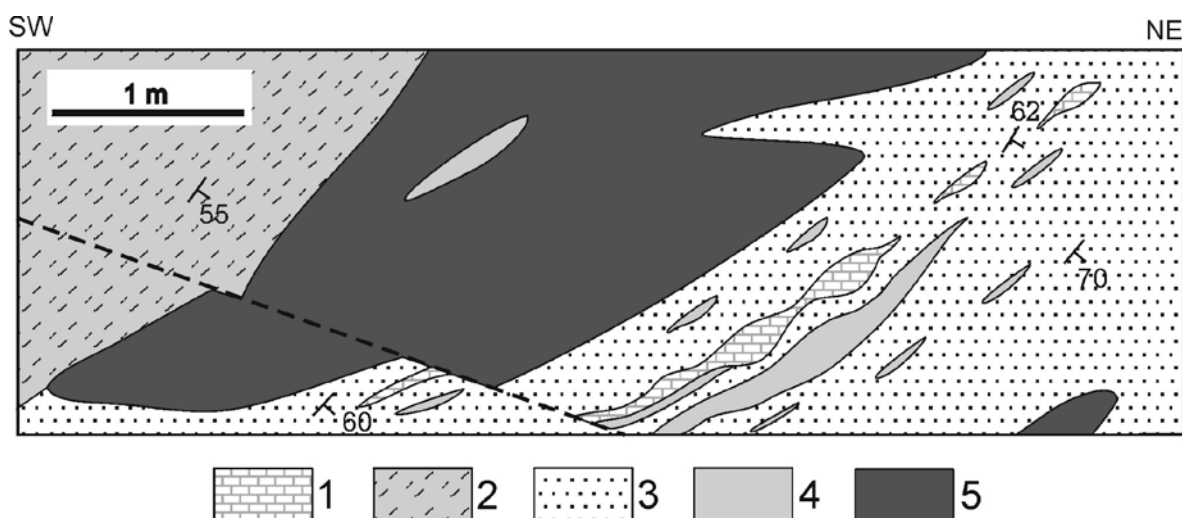
Fig 4: Schematic profile through the Fe-mineralization below the 9th level (Reif 1985). 1-limestone; 2-chlorite-sericite schist; 3-calcareous schist; 4-lenses of sulphides (mainly pyrite); and 5-Fe ores.

Object 2: This is a lensoidal body which occurs in the adit No. 10 824 in the Western Devonian Zone. The body is located below the 9th level and occurs along the border between calcareous schist and chlorite-sericite schist and is associated with low quantities of sulphides. The ore body has an inclination of about 25° to SSW and strikes WNW-ESE (Reif 1985) (Fig. 4). Whereas in the underlying bed magnetite is the dominating ore mineral, the hanging wall is enriched by Fe-Mn-carbonate. The hanging part of the ore body is interlayered with limestone containing Fe-Pb-Zn sulphides. The transcurrent joints occurring within the iron ore body are mineralized with calcite. The samples of object 2 have the label "L".

Object 3: The investigated material is from two borehole samples (HB-906, 364 – 367 m depth and HB-921, 96.5 m depth) occurring in the underlying bed of limestone and hyaloclastite of the Western Devonian Zone.

Samples and methods

The samples are identical with those used for preparation of both the diploma and dissertation theses of J. Reif (1985, 2000a). Whole-rock analyses and trace-element analyses of the ore were carried out in the ACME laboratory (Vancouver, Canada) by the AES-ICP and ICP-MS methods. Trace elements of magnetite and pyrite separates were determined by ICP-MS in the Institute of Analytical Chemistry of the Masaryk University, Brno by I. Novotný & J. Reif and by spectral analysis at the former Institute of Raw Material (Kutná Hora) by M. Kolínský.

The chemical composition of minerals was investigated by electron microprobe CAMECA SX 100 at the Institut für Endlagerforschung of the Technical University of Clausthal-Zellerfeld, Germany (analyst K. Hermann) and at the Masaryk University, Brno (analyst R. Škoda). For quantitative measurement, 15 kV acceleration voltage, 20 nA current on the Faraday cup and 5μm defocused beam were chosen. The PAP matrix correction method for the raw counts was employed (Pouchou & Pichoir 1985).

Isotope analyses of carbon and oxygen in carbonates were conducted at the Czech Geological Survey, Prague (analysts J. Hladíková, I. Jačková & Z. Lněničková). CO_2 was liberated by reaction with 100% orthophosphoric acid and its C and O isotope composition was determined using a Finnigan MAT 251 mass spectrometer. Siderite oxygen data were corrected for isotope fractionation by value of +1.44. Analyses of isotopic composition of sulphur in pyrites were conducted in the same laboratory by J. Hladíková after combustion with CuO at 900 °C. Oxygen for isotopic analyses of magnetite was liberated by a fluorination technique using BrF_5, similar to that of Clayton & Mayeda (1963), at the Institute of Geochemistry, Mineralogy and Mineral Resources, Faculty of Science, Charles University in Prague (M. Pudilová). During this procedure oxygen is cryogenically cleaned from reaction products and excess fluorination agent; finally it is converted to CO_2 on a heated graphite rod. Isotopic measurements were performed using the Finnigan MAT 251 mass spectrometer at the Czech Geological Survey, Prague. The results of all isotope analyses are expressed in standard delta (δ) notation as per mil (‰) deviation from commonly used standards (PDB, SMOW, CDT). Uncertainty limits are: ± 0.05, ± 0.1, ± 0.2, and ± 0.2 ‰ for carbonate $\delta^{13}C$, carbonate $\delta^{18}O$, pyrite $\delta^{34}S$, and magnetite $\delta^{18}O$ values, respectively. The isotopic composition of the parent fluid was calculated using published fractionation factors (O´Neil et al. 1969, Zheng & Simon 1991).

Fluid inclusions were investigated by means of petrography and microthermometry. Inclusions were studied in ~100-μm-thick doubly polished plates. Primary (P), pseudosecondary (PS) and secondary (S) fluid inclusions contained aqueous liquid (L) and vapour (V). Microthermometric parameters were measured using the Linkam THMSG 600 stage mounted on the Olympus BX-51 microscope. The stage was calibrated between – 56.6 and 374.1 °C with inorganic standards and synthetic fluid inclusions. The homogenization temperature (Th), eutectic temperature (Te), temperature of ice melting (Tm_{ice}) and temperature of hydrohalite melting (Tm_{hh}) were measured. All-liquid inclusions were stretched by overheating in order to allow measuring of cryometric parameters. Salinity of the aqueous solution was calculated according to Bodnar (1993).

Calculation of the formulae

The general formula of stilpnomelane is (K, Na,H_3O)$_1$(Fe^{2+},Mg)$_8$ [(OH)$_8$/(Si,Al)$_{12}O_{28}$] • $2H_2O$. The analyses (Tab. 1) were calculated on the basis of 20 and not 21 cations. This is due to the fact that the amount of K, Na and H_3O (including Ca and Ba occurring in Horní Benešov) is unknown. Two cases occur in the procedure of electron neutrality calculation:

1. The sum of the valences of the anions (= 64) is higher than the sum of the valences of the cations (under the assumption that iron is exclusively Fe^{2+}; Tab. 1, columns II – V, VII, and X). The excess of negative charges is compensated by the introduction of a certain amount of Fe^{3+} instead of Fe^{2+}.

2. The sum of the valences of the anions (= 64) is lower than the total of the valences of the cations (under the assumption that iron is exclusively Fe^{2+}; columns I, VI, VIII, IX, and XI). The deficiency of negative charges is compensated by the introduction of O^{2-} instead of OH⁻. As a consequence, Fe^{3+} does not occur.

Tab 1: Selected analyses of stilpnomelane (wt. %; A) and calculated atoms per formula unit (apfu; B)

	Stilpnomelane										
	I	**II**	**III**	**IV**	**V**	**VI**	**VII**	**VIII**	**IX**	**X**	**XI**
	HB-BL 13a	HB-BL 53a	HB-BL 53b	HB-BL 53c	HB-BL 56	HB-BL 53d	HB-BL 55	HB-BL 13b	HB-BL 50	HB-BL 15	HB-906
A: Weight-percent (wt. %)											
SiO_2	45.70	45.63	45.57	45.95	47.26	45.79	45.59	43.98	44.14	46.27	45.75
Al_2O_3	3.94	4.23	4.37	4.41	4.64	4.69	4.88	5.01	5.10	6.79	5.66
FeO_{anal}	36.75	36.20	35.24	35.91	29.51	36.94	35.83	36.77	36.47	31.29	35.52
NiO	-	0.09	0.05	-	-	-	-	-	-	-	-
ZnO	-	-	-	0.06	-	-	-	-	-	-	-
MnO	0.24	0.11	0.13	0.10	0.82	0.10	0.31	0.27	0.15	1.92	0.03
MgO	1.35	1.61	1.65	1.53	5.01	1.76	1.58	1.49	1.16	3.18	2.45
BaO	2.51	2.71	2.12	2.67	3.36	1.63	2.11	2.95	2.03	3.09	0.15
CaO	0.15	0.24	0.38	0.31	0.13	0.23	0.67	0.12	0.18	0.09	0.12
Na_2O	n.d.	0.27	0.14	0.16	0.14	0.06	0.10	0.13	0.10	0.15	0.85
K_2O	0.66	1.01	1.51	0.93	0.45	0.82	0.77	0.87	1.29	0.59	1.33
H_2O^+	4.99	4.92	4.72	4.85	4.97	5.09	4.96	4.98	4.94	5.20	5.14
H_2O^-	2.50	2.50	2.48	2.50	2.56	2.49	2.51	2.49	2.47	2.60	2.57
H_3O	0.65	0.33	0.22	0.41	0.63	0.70	0.47	0.48	0.35	0.63	0.15
FeO_{calc}	36.13	-	-	-	-	34.70	-	34.48	35.37	-	31.34
Fe_2O_{3calc}	0.69	-	-	-	-	2.49	-	2.55	1.22	-	4.65
∑	**99.51**	**99.85**	**98.58**	**99.79**	**99.48**	**100.60**	**99.78**	**98.75**	**98.40**	**101.80**	**100.24**
B: Atoms per formula unit (apfu)											
Si	10.973	10.935	11.007	10.994	11.045	10.784	10.865	10.586	10.700	10.660	10.665
Al	1.027	1.065	0.993	1.006	0.955	1.216	1.135	1.414	1.300	1.340	1.335
∑	*12.000*	*12.000*	*12.000*	*12.000*	*12.000*	*12.000*	*12.000*	*12.000*	*12.000*	*12.000*	*12.000*
Al	0.088	0.130	0.251	0.238	0.323	0.086	0.235	0.008	0.157	0.504	0.219
Fe^{3+}	0.125	-	-	-	-	0.441	-	0.461	0.223	-	0.815
Fe^{2+}	7.255	7.255	7.119	7.186	5.768	6.835	7.141	6.941	7.170	6.029	6.108
Ni	-	0.017	0.010	-	-	-	-	-	-	-	-
Zn	-	-	-	0.010	-	-	-	-	-	-	-
Mn	0.049	0.023	0.026	0.020	0.163	0.020	0.063	0.055	0.031	0.375	0.007
Mg	0.483	0.575	0.594	0.546	1.746	0.618	0.561	0.535	0.419	1.092	0.851
∑	*8.000*	*8.000*	*8.000*	*8.000*	*8.000*	*8.000*	*8.000*	*8.000*	*8.000*	*8.000*	*8.000*
Ba	0.237	0.255	0.200	0.250	0.308	0.150	0.198	0.278	0.190	0.280	0.011
Ca	0.069	0.062	0.099	0.079	0.032	0.058	0.170	0.030	0.094	0.022	0.058
Na	-	0.125	0.065	0.075	0.063	0.027	0.046	0.061	0.047	0.066	0.384
K	0.202	0.308	0.466	0.283	0.135	0.246	0.233	0.268	0.399	0.173	0.396
H_3O	0.492	0.250	0.170	0.313	0.462	0.519	0.353	0.363	0.270	0.459	0.151
∑	*1.000*	*1.000*	*1.000*	*1.000*	*1.000*	*1.000*	*1.000*	*1.000*	*1.000*	*1.000*	*1.000*
OH	8.000	7.868	7.613	7.752	7.754	8.000	7.885	8.000	8.000	7.993	8.000
O	-	0.132	0.387	0.284	0.246	-	0.115	-	-	0.007	-
∑	*8.000*	*8.000*	*8.000*	*8.000*	*8.000*	*8.000*	*8.000*	*8.000*	*8.000*	*8.000*	*8.000*
$∑H_2O$	*2.000*	*2.000*	*2.000*	*2.000*	*2.000*	*2.000*	*2.000*	*2.000*	*2.000*	*2.000*	*2.000*
∑O	*56.000*	*56.000*	*56.000*	*56.000*	*56.000*	*56.000*	*56.000*	*56.000*	*56.000*	*56.000*	*56.000*

Tab 2: Selected analyses of chamosite (wt. %; A), calculated atoms per formula unit (apfu; B) and temperatures of formation (C). (C= Cathelineau; J = Jowett)

Sample	Chamosite (chlorite)									
	I	**II**	**III**	**IV**	**V**	**VI**	**VII**	**VIII**	**IX**	**X**
	L-1	**L-24a**	**L-24b**	**15a**	**15b**	**15c**	**15d**	**15e**	**15f**	**15g**
A: Weight-percent (wt. %)										
SiO_2	26.43	25.97	26.28	27.32	26.00	26.43	26.75	26.03	26.25	26.36
Al_2O_3	18.12	18.49	18.49	17.77	18.61	18.59	18.91	19.14	19.03	19.26
V_2O_3	-	-	0.14	-	-	-	-	-	-	-
FeO_{anal}	37.87	37.56	37.30	35.73	35.96	36.03	35.79	35.90	35.79	33.79
ZnO	-	-	0.08	0.15	-	0.07	-	0.10	-	-
MnO	0.93	0.95	0.78	1.06	0.88	1.03	0.94	0.88	1.25	0.80
MgO	5.98	6.33	6.45	7.08	7.27	7.35	7.44	7.78	7.77	8.11
BaO	-	-	-	0.45	0.21	0.24	0.19	0.10	0.25	0.59
CaO	-	-	-	0.11	0.12	0.08	0.12	0.08	0.09	-
Na_2O	0.07	0.08	-	0.05	-	-	-	-	-	0.06
K_2O	-	-	-	0.17	-	-	-	-	-	-
H_2O_{calc}	10.31	10.46	10.35	10.37	10.45	10.54	10.47	10.67	10.69	10.39
Σ	**99.71**	**100.02**	**99.87**	*100.26*	**99.50**	**100.42**	**100.61**	**100.68**	**101.12**	*99.36*
B: Atoms per formula unit (apfu)										
Si	2.940	2.896	2.929	3.026	2.896	2.915	2.938	2.856	2.870	2.915
Al	1.060	1.104	1.071	0.974	1.104	1.085	1.062	1.144	1.130	1.085
Σ	*4.000*	*4.000*	*4.000*	*4.000*	*4.000*	*4.000*	*4.000*	*4.000*	*4.000*	*4.000*
Al	1.331	1.325	1.358	1.345	1.338	1.332	1.386	1.331	1.323	1.425
V	-	-	0.013	-	-	-	-	-	-	-
Fe	3.547	3.501	3.476	3.309	3.349	3.325	3.287	3.293	3.273	3.125
Mn	0.088	0.090	0.074	0.099	0.083	0.096	0.088	0.082	0.116	0.075
Zn	-	-	0.007	0.012	-	0.006	-	0.008	-	-
Mg	0.998	1.051	1.072	1.168	1.207	1.208	1.217	1.272	1.266	1.337
Ba	-	-	-	0.019	0.009	0.011	0.008	0.005	0.011	0.025
Ca	-	-	-	0.013	0.014	0.009	0.014	0.009	0.011	-
Na	0.016	0.017	-	0.011	-	-	-	-	-	0.013
K	-	-	-	0.024	-	-	-	-	-	-
Σ	*6.000*	*6.000*	*6.000*	*6.000*	*6.000*	*6.000*	*6.000*	*6.000*	*6.000*	*6.000*
O	0.295	0.220	0.300	0.336	0.234	0.234	0.324	0.187	0.193	0.327
OH	7.705	7.780	7.700	7.664	7.766	7.766	7.676	7.813	7.807	7.673
Σ	*8.000*	*8.000*	*8.000*	*8.000*	*8.000*	*8.000*	*8.000*	*8.000*	*8.000*	*8.000*
Σ O	*10.000*	*10.000*	*10.000*	*10.000*	*10.000*	*10.000*	*10.000*	*10.000*	*10.000*	*10.000*
C: Temperature of formation (^{o}C)										
C	279.3	283.6	282.9	251.7	293.5	287.4	280.0	306.4	301.9	287.4
J	294.0	307.7	297.0	265.8	306.6	300.5	293.1	318.9	314.5	299.4

Tab 3: Selected analyses of berthierine (wt. %; A) and calculated atoms per formula unit (apfu; B).

	Berthierine								
	I	**II**	**III**	**IV**	**V**	**VI**	**VII**	**VIII**	**IX**
Sample	HB-906a	BL-6	L-14a	L-14b	HB-906b	HB-906c	HB-906d	HB-906e	HB-906f
A: Weight-percent (wt. %)									
SiO_2	29.69	27.32	27.29	27.70	27.24	26.79	26.72	26.47	26.38
TiO_2	2.86	0.04	-	-	0.19	0.16	0.23	0.05	n.d.
Al_2O_3	7.93	11.33	11.95	12.93	13.17	14.72	15.10	15.32	15.42
V_2O_3	0.19	-	-	-	0.17	0.16	0.12	0.12	0.17
Cr_2O_3	0.04	-	-	-	-	-	-	0.06	0.05
FeO_{anal}	46.19	48.70	48.26	48.31	44.37	42.85	41.99	42.56	42.95
NiO	-	-	-	-	-	0.05	0.04	-	-
ZnO	-	-	-	-	-	-	-	-	0.06
MnO	0.10	0.31	0.50	0.44	0.05	0.05	-	-	-
MgO	2.35	0.55	0.45	0.51	3.79	4.52	4.51	4.52	4.49
BaO	-	0.04	-	-	-	-	-	-	-
CaO	0.16	-	-	-	0.08	0.21	0.42	0.30	0.25
Na_2O	-	-	-	-	-	0.10	0.13	0.05	-
H_2O_{calc}	9.43	9.69	9.57	9.66	10.07	10.33	10.27	10.31	10.36
Σ	**98.94**	**98.12**	**98.02**	**99.55**	**99.13**	**99.94**	**99.53**	**99.76**	**100.13**
B: Atoms per formula unit (apfu)									
Si	3.544	3.300	3.295	3.279	3.171	3.063	3.058	3.028	3.008
Al	0.456	0.700	0.705	0.721	0.829	0.937	0.942	0.972	0.992
Σ	*4.000*	*4.000*	*4.000*	*4.000*	*4.000*	*4.000*	*4.000*	*4.000*	*4.000*
Ti	0.771	0.004	-	-	0.017	0.014	0.020	0.004	-
Al	0.660	0.912	0.995	1.083	0.977	1.047	1.095	1.093	1.081
V	0.054	-	-	-	0.016	0.014	0.011	0.011	0.016
Cr	0.012	-	-	-	-	-	-	0.005	0.005
Fe	4.612	4.918	4.873	4.783	4.318	4.098	4.020	4.070	4.098
Ni	-	-	-	-	-	0.005	0.003	-	-
Mn	0.020	0.032	0.051	0.044	0.005	0.005	-	-	-
Zn	-	-	-	-	-	-	-	-	0.005
Mg	0.418	0.099	0.081	0.090	0.657	0.770	0.770	0.770	0.764
Ba	-	0.002	-	-	-	-	-	-	-
Ca	0.042	-	-	-	0.010	0.025	0.052	0.036	0.031
Na	-	-	-	-	-	0.022	0.029	0.011	-
Σ	*6.000*	*6.000*	*6.000*	*6.000*	*6.000*	*6.000*	*6.000*	*6.000*	*6.000*
O	0.483	0.183	0.290	0.362	0.181	0.116	0.155	0.130	0.110
OH	7.517	7.817	7.710	7.638	7.819	7.884	7.845	7.870	7.890
Σ	*8.000*	*8.000*	*8.000*	*8.000*	*8.000*	*8.000*	*8.000*	*8.000*	*8.000*
Σ O	*10.000*	*10.000*	*10.000*	*10.000*	*10.000*	*10.000*	*10.000*	*10.000*	*10.000*

Tab 4: Selected analyses of odinite (containing 6 OH groups only) (wt. %; A) and calculated atoms per formula unit (apfu; B).

		Odinite (with 6 OH)								
	I	**II**	**III**	**IV**	**V**	**VI**	**VII**	**VIII**	**IX**	**X**
Sample	HB-BL-63	HB-BL-41	HB-BL-58a	HB-BL-58b	HB-612	HB-BL-48a	HB-BL 48b	HB-L-6	HB-BL 15a	HB-BL 15b
A: Weight- percent (wt. %)										
SiO_2	37.08	35.60	35.43	34.73	35.51	34.63	34.52	33.70	37.64	33.29
Al_2O_3	0.09	0.86	1.63	1.95	2.62	5.60	6.19	7.48	11.73	14.58
FeO_{anal}	51.46	54.11	51.72	51.57	51.92	47.33	46.48	49.44	33.92	35.18
MnO	1.14	0.27	0.90	1.05	0.05	0.18	0.22	0.34	1.45	1.25
MgO	1.36	0.79	1.46	1.38	1.02	2.40	2.59	0.48	5.27	6.28
BaO	0.09	-	-	-	-	-	0.21	0.08	1.35	0.86
CaO	-	-	-	0.13	0.66	0.25	0.19	0.04	0.10	0.09
Na_2O	0.06	-	-	-	-	0.04	0.08	0.06	0.13	-
K_2O	0.05	-	-	-	0.05	-	0.15	-	0.45	0.19
FeO_{calc}	51.34	51.94	49.93	48.90	50.65	47.33	46.48	49.44	33.92	35.18
Fe_2O_{3calc}	0.14	2.41	1.99	2.97	1.41	-	-	-	-	-
H_2O_{calc}	8.33	8.32	8.34	8.31	8.43	8.43	8.52	8.41	7.56	8.69
Σ	**99.68**	**100.19**	**99.68**	**99.42**	**100.40**	**98.86**	**99.15**	**100.03**	**99.60**	**100.41**
B: Atoms per formula unit (apfu)										
Si	**4.000**	**3.847**	**3.816**	**3.755**	**3.789**	**3.672**	**3.641**	**3.567**	**3.748**	**3.293**
Al	-	0.110	0.184	0.245	0.211	0.328	0.359	0.433	0.252	0.707
Σ	*4.000*	*3.957*	*4.000*	*4.000*	*4.000*	*4.000*	*4.000*	*4.000*	*4.000*	*4.000*
Al	0.012	-	0.023	0.004	0.118	0.371	0.409	0.500	1.125	0.993
Fe^{3+}	0.011	0.196	0.161	0.241	0.113	-	-	-	-	-
Fe^{2+}	4.632	4.695	4.500	4.422	4.520	4.197	4.098	4.376	2.825	2.910
Mn	0.104	0.025	0.082	0.096	0.004	0.016	0.020	0.031	0.122	0.105
Mg	0.218	0.127	0.234	0.222	0.162	0.379	0.406	0.076	0.782	0.925
Ba	0.004	-	-	-	-	-	0.009	0.001	0.053	0.033
Ca	-	-	-	0.015	0.076	0.029	0.022	0.004	0.011	0.010
Na	0.012	-	-	-	-	0.008	0.016	0.012	0.025	-
K	0.007	-	-	-	0.007	-	0.020	-	0.057	0.024
Σ	*5.000*	*5.043*	*5.000*	*5.000*	*5.000*	*5.000*	*5.000*	*5.000*	*5.000*	*5.000*
OH	**6.000**	**6.000**	**6.000**	**6.000**	**6.000**	**5.969**	**5.989**	**5.945**	**5.029**	**5.738**
O	**-**	**-**	**-**	**-**	**-**	**0.031**	**0.011**	**0.055**	**0.971**	**0.262**
Σ	*6.000*	*6.000*	*6.000*	*6.000*	*6.000*	*6.000*	*6.000*	*6.000*	*6.000*	*6.000*
Σ O	*10.000*	*10.000*	*10.000*	*10.000*	*10.000*	*10.000*	*10.000*	*10.000*	*10.000*	*10.000*

The amount of 8 (OH) = $4H_2O + 4O = (H_2O)^+$; $2 H_2O (= H_2O)^-$; and H_3O (determined by difference) were calculated according to the formula, transformed into wt. % and added to the analytical results.

Chlorite (Tab. 2) and berthierine (Tab. 3) analyses were calculated on the basis of 10 cations including minor CaO, Na_2O and K_2O. The calculation procedure of electron neutrality for the chlorite formula $(Fe^{2+},Mg,Fe^{3+},Al)_6[OH]_8/(Si,Al)_4O_{10}]$ is based on the fact that the sum of the valences of the anions (= 28) is lower than the total of the valences of the cations (under the assumption that iron is exclusively Fe^{2+}). The deficiency of negative charges is compensated by the introduction of O^{2-} instead of OH^-. As a consequence, Fe^{3+} does not occur. The amount of $(OH)_{8-x}$ (in mol. %) is converted into wt. % as H_2O and added to the analytical sum.

Odinite (Tab. 4) with the formula of $(Fe^{2+},Mg,Al)_5[(OH)_6/(Si,Al)_4O_{10}]$ is calculated on the basis of 9 cations. The calculation procedure in order to achieve electron neutrality is the following:

1. The sum of the valences of the anions (= 26) is higher than the sum of the valences of the cations (under the assumption that iron is Fe^{2+}; columns I - V). The excess of negative charges is compensated by the introduction of a certain amount of Fe^{3+}.

2. The sum of the valences of the anions (= 26) is lower than the total of the valences of the cations (under the assumption that iron is exclusively Fe^{2+}; columns VI - X). The deficiency of negative charges is compensated by the introduction of O^{2-} instead of OH^-. As a consequence, Fe^{3+} does not occur.

The amount of $(OH)_6$ (in mol. %) is converted into wt. % as $H_2O^+ (= 3H_2O)$ and added to the analytical sum.

Carbonate analyses were calculated on the basis of one cation (Ca + Fe + Mn + Mg = 1) for the calcite group and for that of dolomite on the basis of two cations (Ca + Fe + Mn + Mg = 2). Deduced from the formulae of both calcite (Tab. 5, 6 and 7, columns I – VI) and dolomite (Tab. 7, columns VII-X) groups, equivalent proportions of CO_2 were calculated, transformed into wt. % and added to the analytical sum. The calculated values of the cations (in at. %) are not published, but the values of the corresponding end-members (in mol. %).

The formulae of magnetite (Tab. 8) were calculated on the basis of three cations. The calculated values are not published, but the corresponding abundances of end-members (mol. %). The amount of Fe^{2+} and Fe^{3+} were transformed into wt. % (expressed as FeO_{calc} and Fe_2O_{3calc}) and added to the analytical sum instead of FeO_{anal}.

The analytical data (in wt. %) of the sulphides were calculated into atomic percent (at. %). The calculation procedure depends on the formula of the investigated minerals [e. g. sphalerite (Tab. 9): $\Sigma(Zn + Fe + Mn + Co + Ag) = 1 : \Sigma(S + As) = 1$].

Tab 5: Selected analyses of calcite (wt. %; A) and calculated end-member concentrations (mol. %; B). The apfu-data from which the end-member concentrations were calculated, are not presented.

	Calcite solid solutions										
	I	**II**	**III**	**IV**	**V**	**VI**	**VII**	**VIII**	**IX**	**X**	**XI**
A: Weight-percent (wt. %)											
CaO	53.04	52.73	50.75	50.28	49.39	48.79	50.75	49.37	49.29	47.85	46.59
MgO	0.41	0.38	0.42	0.44	0.25	0.47	0.25	0.72	0.28	0.29	0.22
FeO	2.43	2.20	4.86	3.12	5.90	6.34	0.75	4.39	1.90	4.32	1.91
MnO	0.28	0.29	0.04	0.49	0.16	0.49	4.38	2.57	5.18	2.47	7.81
SrO	1.30	0.65	1.01	1.29	1.76	1.06	0.83	0.58	0.62	2.05	0.10
CO$_{2cal.}$	44.28	43.60	43.72	44.20	43.58	44.20	43.63	44.10	43.62	42.91	42.87
Σ	*101.74*	*99.85*	*100.80*	*99.82*	*101.04*	*99.82*	*100.59*	*101.73*	*100.89*	*99.89*	*99.50*
B: Mol-percent (mol. %)											
CaCO$_3$	94.00	94.91	91.10	89.28	89.11	88.13	91.29	87.85	88.67	87.50	85.29
MgCO$_3$	1.01	0.95	1.05	1.09	0.63	1.19	0.63	1.79	0.70	0.74	0.57
FeCO$_3$	3.36	3.09	6.81	7.71	8.31	8.94	1.05	6.19	2.66	6.16	2.73
MnCO$_3$	0.39	0.41	0.06	0.69	0.23	0.70	6.22	3.61	7.36	3.57	11.31
SrCO$_3$	1.24	0.64	0.98	1.23	1.72	1.04	0.81	0.56	0.61	2.03	0.10

Tab 6: Selected analyses of siderite (wt. %; A) and calculated end-member concentrations (mol. %; B). The apfu-data from which the end-member concentrations were calculated, are not presented.

	Siderite solid solutions									
	I	**II**	**III**	**IV**	**V**	**VI**	**VII**	**VIII**	**IX**	**X**
A: Weight-percent (wt. %)										
CaO	1.25	9.54	0.08	1.05	4.38	1.36	2.41	1.11	0.38	0.90
MgO	4.77	5.13	9.34	0.27	0.69	1.21	3.12	1.85	1.79	0.86
FeO	30.94	39.95	49.37	52.75	53.61	53.68	54.54	58.37	58.40	58.90
MnO	22.49	4.43	0.82	7.53	2.27	5.37	0.60	0.04	1.61	0.69
CO$_{2cal.}$	39.09	40.30	41.01	38.10	38.44	38.60	39.08	38.67	39.02	38.15
Σ	*98.54*	*99.35*	*100.62*	*99.70*	*99.39*	*100.22*	*99.75*	*100.04*	*101.20*	*99.50*
B: Mol-percent (mol. %)										
CaCO$_3$	2.51	18.57	0.15	2.16	8.94	2.77	4.84	2.25	0.77	1.85
MgCO$_3$	13.32	13.90	24.86	0.77	1.96	3.42	8.72	5.22	5.01	2.46
FeCO$_3$	48.48	60.72	73.74	84.81	85.44	85.18	85.48	92.46	91.66	94.57
MnCO$_3$	35.69	6.81	1.25	12.26	3.66	8.63	0.96	0.07	2.56	1.12

Tab 7: Selected analyses of rhodochrosite, dolomite and ankerite (wt. %; A) and calculated end-member concentrations (mol. %; B). Dolomite and ankerite are presented under (B) according to the calcite-type for comparison (upper part) and to the dolomite-type (lower part). The apfu-data from which the end-member concentrations were calculated, are not presented.

	Rhodochrosite solid solutions						Dolomite/ankerite solid solutions			
	I	**II**	**III**	**IV**	**V**	**VI**	**VII**	**VIII**	**IX**	**X**
A: Weight-percent (wt. %)										
CaO	6.12	1.65	0.25	0.27	1.12	0.79	28.09	26.75	30.34	29.65
MgO	0.54	0.68	0.07	0.15	1.00	0.09	7.40	7.14	21.33	22.04
FeO	10.53	13.73	10.56	9.60	4.48	n. d.	15.44	17.87	1.42	1.24
MnO	43.55	45.20	50.56	51.08	54.55	61.17	5.42	4.69	0.07	n. d.
ZnO	-	0.07	-	-	-	-	-	-	-	0.06
SrO	-	-	-	-	-	-	0.20	0.16	-	-
CO$_{2cal}$	38.82	38.53	38.11	37.95	38.56	38.66	43.03	42.70	48.01	48.12
Σ	*99.56*	*99.86*	*99.55*	*99.05*	*99.71*	*100.71*	*99.58*	*99.51*	*101.17*	*101.11*
B: Mol-percent (mol. %)										
CaCO$_3$	12.37	3.36	0.52	0.55	2.28	1.60	51.24	49.15	49.59	48.35
MgCO$_3$	1.52	1.93	0.20	0.43	2.83	0.24	18.78	18.25	48.50	50.00
FeCO$_3$	16.62	21.83	16.98	15.50	7.12	-	21.98	25.63	1.82	1.58
MnCO$_3$	69.49	72.78	82.30	83.52	87.77	98.16	7.81	6.81	0.09	-
ZnCO$_3$	-	0.10	-	-	-	-	-	-	-	0.07
SrCO$_3$	-	-	-	-	-	-	0.19	0.16	-	-
Σ	*100.0*	*100.0*	*100.0*	*100.0*	*100.0*	*100.0*	*100.0*	*100.0*	*100.0*	*100.0*
CaMg(CO$_3$)$_2$	-	-	-	-	-	-	37.56	36.50	95.36	93.54
CaFe(CO$_3$)$_2$	-	-	-	-	-	-	43.96	48.18	3.64	3.16
CaMn(CO$_3$)$_2$	-	-	-	-	-	-	15.62	13.62	0.18	-
FeCO$_3$	-	-	-	-	-	-	-	1.54	-	-
CaCO$_3$	-	-	-	-	-	-	2.67	-	-	-
MgCO$_3$	-	-	-	-	-	-	-	-	0.82	3.23
SrCO$_3$	-	-	-	-	-	-	0.19	0.16	-	-
ZnCO$_3$	-	-	-	-	-	-	-	-	-	0.07
Σ	*100.0*	*100.0*	*100.0*	*100.0*	*100.0*	*100.0*	*100.0*	*100.0*	*100.0*	*100.0*

Tab 8: Selected analyses of magnetite (wt. %; A) and calculated end-member concentrations (mol. %; B). The apfu-data from which the end-member concentrations were calculated, are not presented.

	Magnetite					
	I	**II**	**III**	**IV**	**V**	**VI**
	BL-612		Hb-Py1	BL - 41	HB-BL 60	HB-BL 63
A: Weight-percent (wt.%)						
FeO	91.01	91.77	91.92	92.02	92.10	92.92
SiO_2	2.75	-	0.51	1.98	0.69	1.13
TiO_2	-	0.07	-	-	-	-
Al_2O_3	0.19	0.71	-	-	0.08	0.02
Cr_2O_3	0.03	-	-	-	0.03	-
V_2O_3	-	-	0.10	-	-	-
NiO	-	-	-	-	0.02	-
MnO	-	0.09	0.04	-	0.03	0.11
MgO	0.10	0.06	-	-	-	-
ZnO	0.06	-	0.08	0.03	0.13	-
CaO	0.07	-	0.09	-	0.07	-
Fe_2O_{3cal}	62.67	67.69	67.31	64.69	68.08	66.90
FeO_{cal}	34.61	30.86	31.35	33.80	30.83	32.72
Σ	**100.48**	**99.48**	**99.48**	**100.50**	**99.96**	**100.88**
B: Mol-percent (mol. %)						
$Fe^{2+}Fe^{3+}_2O_4$	88.15	97.50	97.15	92.40	97.55	95.35
$MnFe^{3+}_2O_4$	-	0.30	0.10	-	0.10	0.30
$MgFe^{3+}_2O_4$	0.60	0.40	-	-	-	-
$ZnFe^{3+}_2O_4$	0.10	-	0.20	0.10	0.40	-
$CaFe^{3+}_2O_4$	0.30	-	0.40	-	0.30	-
$Fe^{2+}_2TiO_4$	-	0.20	-	-	-	-
$Fe^{2+}_2SiO_4$	10.40	-	2.00	7.50	1.30	4.30
$Fe^{2+}Al_2O_4$	0.40	1.60	-	-	0.20	0.05
$Fe^{2+}Cr_2O_4$	0.05	-	-	-	0.05	-
$Fe^{2+}V_2O_4$	-	-	0.15	-	-	-

Results

The minerals of the iron ores

Generally, the minerals (especially the Fe-silicates) are extremely fine-grained and therefore, the identification of various silicates by means of polarizing microscopy is almost impossible. This is the reason that the description and the identification of the minerals are often based on observations carried out by an electron microscope.

The following minerals were detected: Fe-silicates (stilpnomelane, odinite, chlorite, and berthierine), magnetite, quartz (including jaspilite = fine-grained mixture of quartz and hematite), carbonates (calcite, siderite, rhodochrosite, ankerite and dolomite), apatite, krauskopfite, barite, scheelite and sulphides (pyrite, sphalerite, galena, chalcopyrite, arsenopyrite, cobaltite, pyrrhotite and a mineral of the linneite group with unsual chemical composition).

Magnetite occurs in most of the sections in quantities normally higher than 30 vol. % (ore type I). In some sections magnetite is of low abundance (up to 5 vol. %, ore type II). Generally, the other minerals (stilpnomelane, odinite and siderite) of both ore types occur in quantities higher than 20 vol. %. Calcite and quartz are of lower abundance and occur in varying proportions. Rare minerals are chlorite, berthierine and rhodochrosite, occurring in quantities higher than 20 vol. %, but only in local restricted domains. Rare minerals occurring

in the form of disseminations are ankerite, dolomite, sulphides, apatite, krauskopfite and barite. Extremely rare accessory in magnetite ore is scheelite.
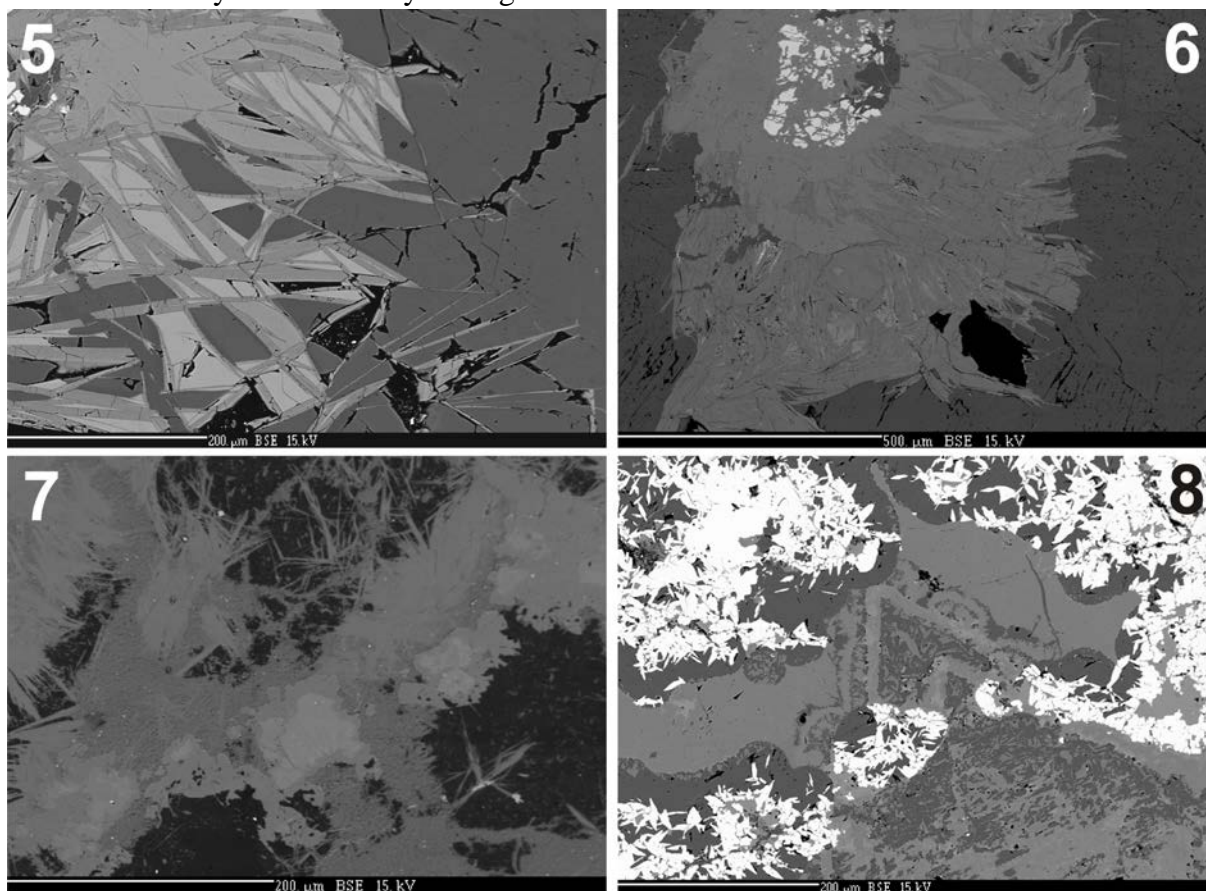

Figs 5-8: 5- Elongated stilpnomelane intergrows with siderite (grey) and odinite (lightgrey) embedded in calcite (dark). Holes are black. BSE photo. BL-63. **6-** Compact aggregate consisting of stilpnomelane, siderite (slightly brighter) and subordinate magnetite (white) enveloped by calcite. BSE photo. BL-63. **7 -** Compact and elongated stilpnomelane partially replaced by chlorite (slightly darker) and zoned rhodochrosite. Quartz is black. BSE photo. L-15. **8-** Rhodochrosite (relatively bright) and calcite (grey) which contains magnetite often rice-grain shaped. Inclusions in magnetite (of the right side) consist of odinite (slightly brighter than rhodochrosite). BSE photo. BL-58.

The groundmass of the two ore types (with and nearly without magnetite) consists of carbonate and Fe-silicates often in proportions of about 1 : 1. The silicates are represented mainly by stilpnomelane and odinite. Stilpnomelane occurs in the form of needle-like crystals (length up to several mm; Fig. 5), but also in compact polycrystalline aggregates often together with siderite (Fig. 6) and odinite (Fig. 5). Stilpnomelane may also occur in postmetamorphic veins in which elongated crystals are arranged parallel to each other and perpendicular to the vein wall (ladder-like texture), together with carbonate. It was also observed in intergrowths with galena in a calcite lens hosted by a fine-grained pyrite-stilpnomelane mixture. Berthierine is rare and occurs closely intergrown with chlorite (Fig. 7). Siderite is the main carbonate mineral, whereas rhodochrosite is restricted to local enrichments in the form of coarse-grained aggregates often showing zonation (Fig. 8) or in recrystallized masses representing originally collomorphic precipitations. Calcite is more abundant than rhodochrosite. It occurs in nearly every sample. Calcite may be coarse-grained often showing corroded grain boundaries (Fig. 9) or resembling brecciated material (diameter up to 400 µm) that may contain inclusions of stilpnomelane (Fig. 10). Calcite also occurs in

the form of recrystallized former collomorphic masses which characteristically include rice-grain shaped magnetite crystals (Fig. 11). Calcite is often included in siderite (Fig. 11).
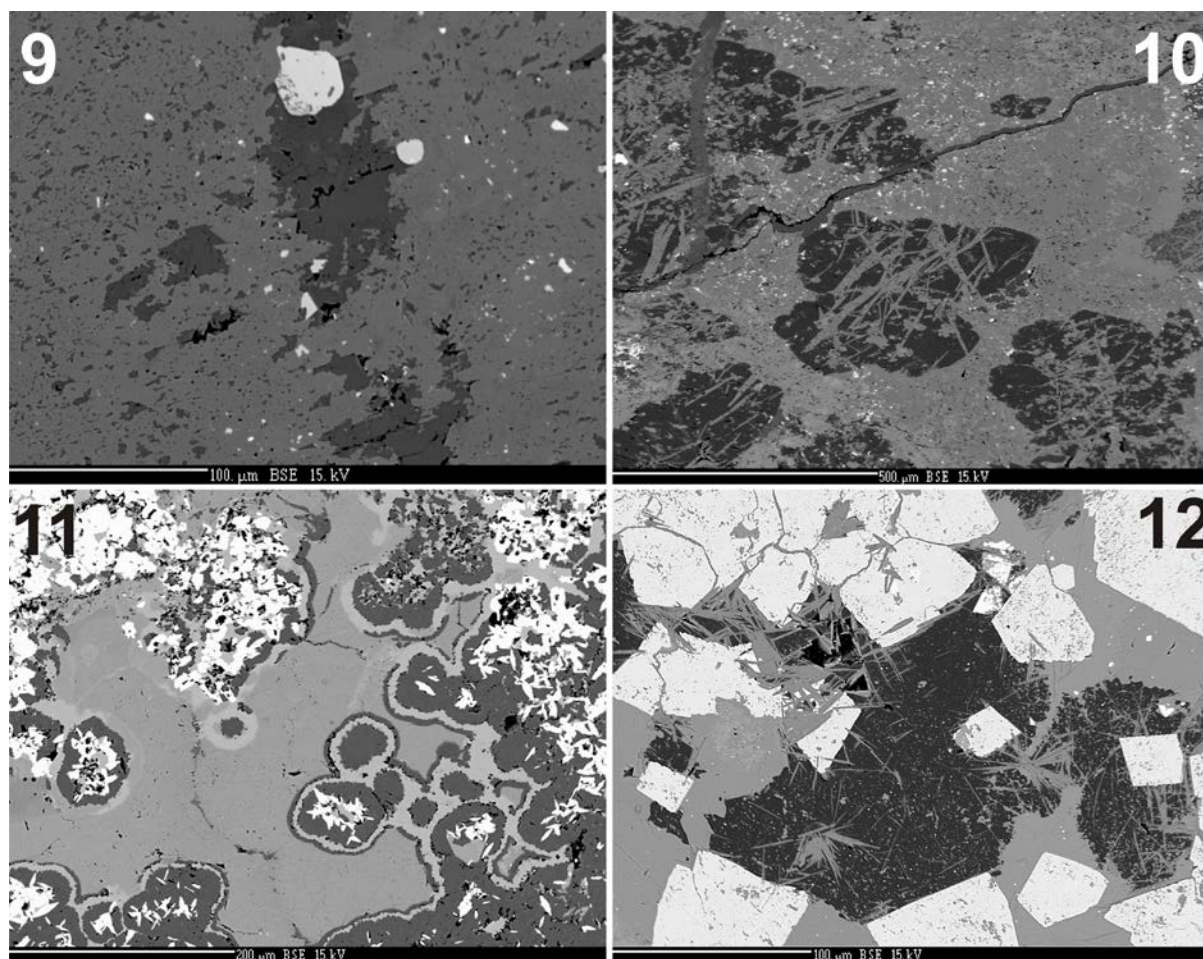

Figs 9-12: **9 -** Corroded relics of calcite in siderite. White are magnetite crystals. BSE photo. HB-BL-63. **10 –** Corroded clasts of calcite intergrown with stilpnomelane in a groundmass of siderite. BSE photo. BL-40. **11 -** Collomorphic intergrowth of calcite (dark) containing rice-grain shaped magnetite and Mn-rich siderite (light grey). The inner calcite zone (containing magnetite) and the outer calcite rim (which grades directly into siderite) is connected by a small zone consisting of odinite. BSE photo. BL-58. **12 -** Idiomorphic magnetite crystals containing tiny siderite and elongated stilpnomelane inclusions are enveloped in siderite and quartz (black). BSE photo. L-6B.

Opaque minerals are predominantly magnetite, subordinate pyrite, rarely sphalerite, arsenopyrite, galena, chalcopyrite and exceptionally also pyrrhotite. Magnetite forms often idioblastic crystals (from 0.03 to 3 - 4 mm in diameter) that contain tiny irregularly shaped inclusions of siderite (Fig. 12). Rarely, magnetite porphyroblasts may also show irregular grain boundaries. Hypidiomorphic magnetite crystals are not as abundant as the idiomorphic types. Magnetite is also developed as lensoidal crystals similar to a rice grain (length up to 20 μm). Rice-grain shaped magnetite may be concentrated in polycrystalline aggregates (Fig. 11). Magnetite which is of minor abundance represents globular-rounded aggregates and irregular ribbon-like forms with tabular crystals. A clear layering of magnetite was not observed. Pyrite (mainly 2-3 vol. %) is developed in various types that occur as xenomorphic relics within magnetite, in form of idioblasts that may contain tiny arsenopyrite inclusions (Fig. 13) and along grain boundaries of magnetite or other associated minerals. Accessory arsenopyrite, often forming triplets, is hosted by siderite cement. In exceptions, polycrystalline masses of pure pyrite take up to 50 vol. % (= ore type III). In comparison with

magnetite, hematite is a very rare mineral. It occurs in the form of finely dispersed pigment in quartz (= jaspilite or ferruginuous quartz; Fig. 14) and carbonates, visible in reflected and transmitted light, respectively, by the abundance of red internal reflections. Compact hematite crystal or polycrystalline hematite aggregates similar to magnetite were not found. Barite is very rare, coarse-grained and intergrown with siderite and stilpnomelane at the locality "L". Apatite forms needle-like crystals (length up to 50 μm) occurring in calcite and associated with stilpnomelane, siderite and magnetite at the locality "BL". The rare krauskopfite forms irregularly shaped aggregates in stilpnomelane (Fig. 15) which are associated with magnetite. Rare scheelite is intergrowthn with stilpnomelane and magnetite which may be corroded.

Fragments of fossils can be also observed, including relics of sponges, trilobites, crinoids and shells of brachiopods (J. Hladil, personal communication). Although Kretschmer (1917, 1918), Karrenberg-Metz & Quitzow (1942) and Skácel (e.g. 1960, 1966) described ooids in Fe-deposits located in the vicinity of Horní Benešov, no ooids were observed in our material.
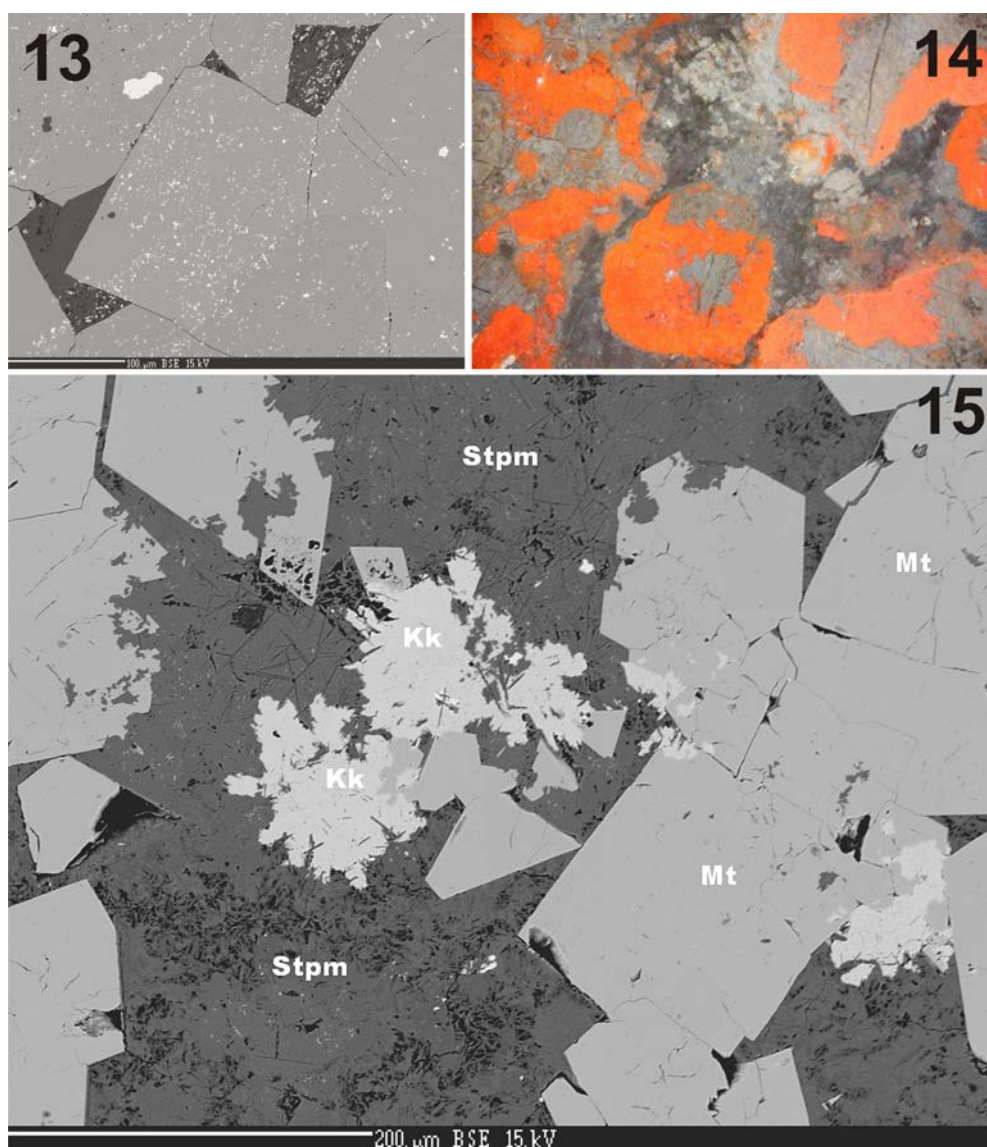
Figs 13-15: 13 - Pyrite idioblasts containing fine-grained arsenopyrite crystals. The space between pyrite crystals is filled by stilpnomelane, minor siderite and tiny arsenopyrite crystals. The latter are distributed in the same size and arrangement in the neighbouring pyrite. BSE photo. BL-44. 14 - Ferruginuous quartz (mixture of fine grained quartz and hematite) with red internal reflections replaced by siderite-rich carbonate. Transmitted light, L-20. 15 - Idiomorphic magnetite crystals (Mt) in a groundmass consisting of stilpnomelane (Stpm), relics of calcite (nearly black) and irregularly shaped aggregates of krauskopfite (Kk slightly brighter than magnetite). BSE photo. BL-53.

230
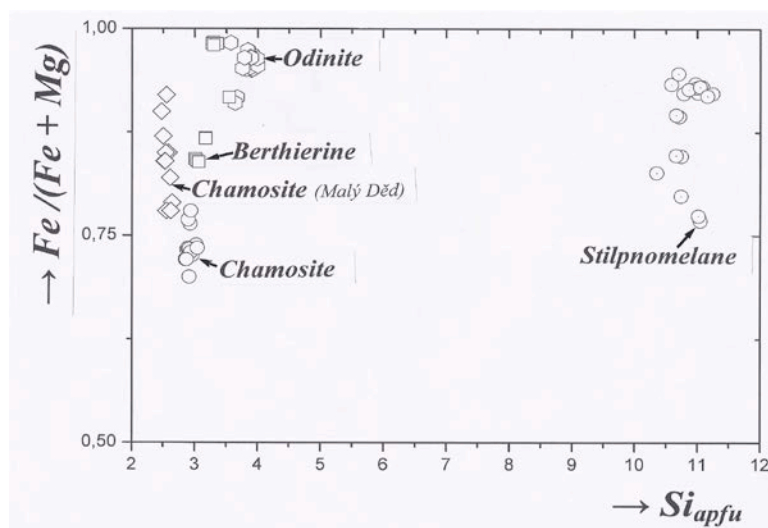
Fig 16: Si_{apfu}-Fe/(Fe + Mg) diagram and the analytical plots of stilpnomelane (circles on the right side) in comparison with those of odinite (hexagon), berthierine (quadrangle) and chamosite of Horní Benešov (circle) and of Malý Děd (rhomb).
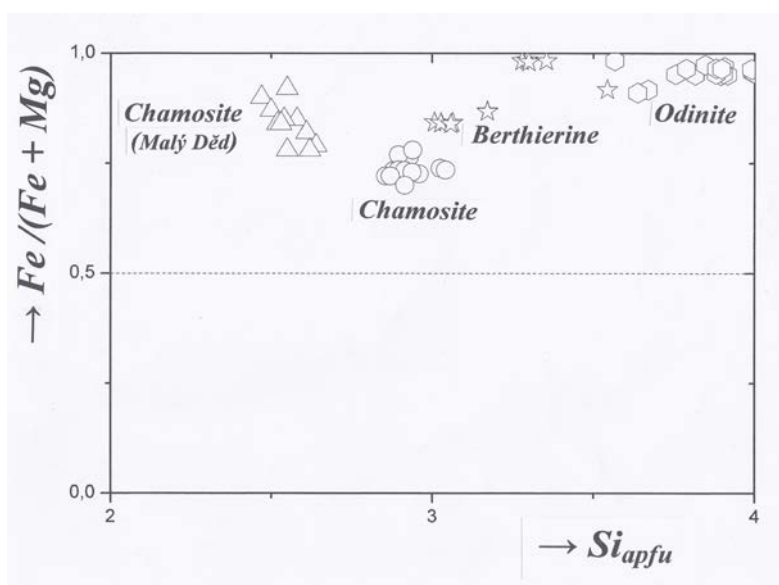

Fig 17: Si_{apfu}-Fe/(Fe + Mg) diagram and the analytical plots of odinite (hexagon), berthierine (star) and chamosite of Horní Benešov (circle) and of Malý Děd (triangle).
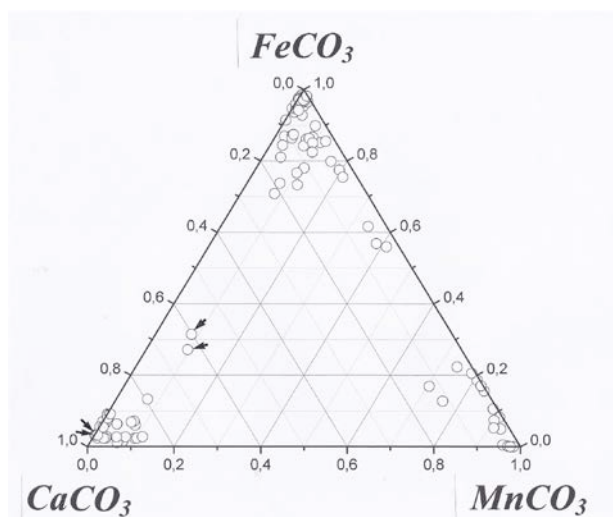

Fig 18: $MnCO_3$ - $FeCO_3$ - $CaCO_3$ diagram of 102 analytical plots of rhodochrosite (17 analyses), siderite (48 analyses), calcite (33 analyses), dolomite (2 analyses; arrowed from the left side) and ankerite (2 analyses; arrowed from the right side).

231
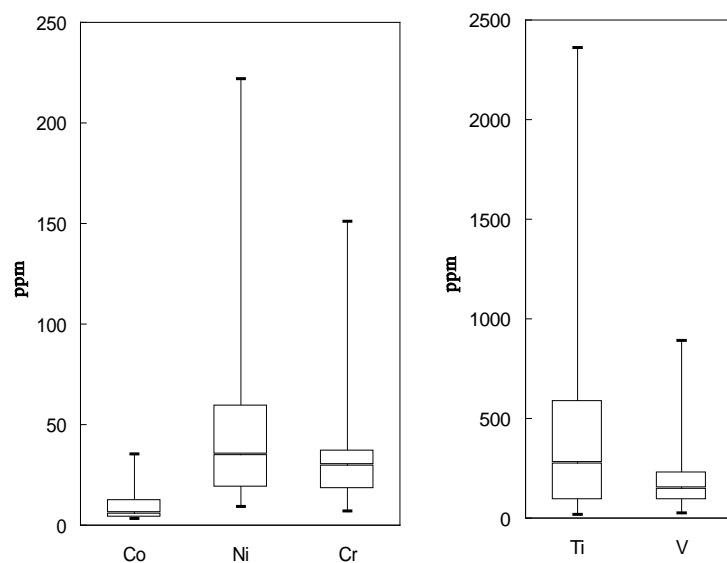
Fig 19: The contents of selected refractory elements of the magnetites.
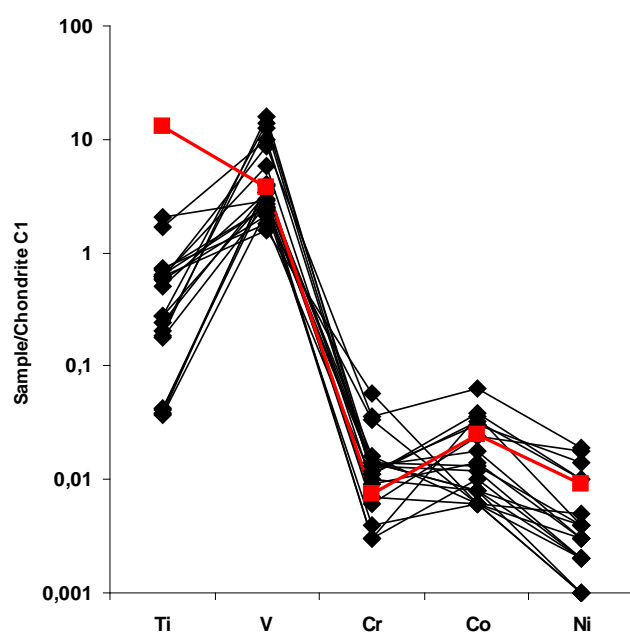
Fig 20: A comparison of magnetite chemistry with an average tholeiitic basalt (after Wedepohl 1975).
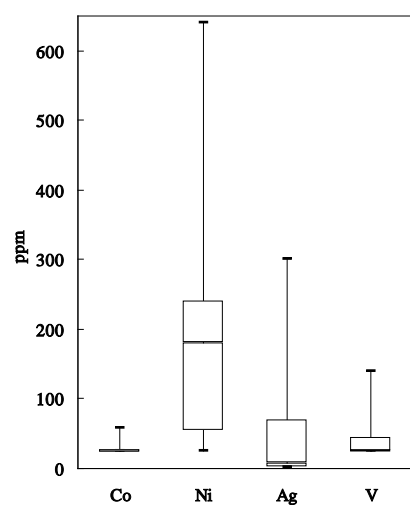
Fig 21: The contents of selected trace elements of the pyrites.

Mineral chemistry

SILICATES

Four Fe-silicates were investigated in this study. Their analytical data are visualized in Fig. 23. This diagram shows that the Fe/(Fe + Mg) ratios range between 0.75 and 1.00. The Si_{apfu} values divide the silicates into two groups. One group has low Si_{apfu} (2.5 - 4) and comprises chamosite, berthierine, and odinite. The other group (Si_{apfu} is about 11) contains stilpnomelane only.

Stilpnomelane: More than 50 analyses of stilpnomelane were carried out and 20 of them are presented in Fig. 16 of which 11 were selected for Tab. 1. In A (upper part of the table) the results are in wt. % including the calculated values of FeO, Fe_2O_3, H_2O^+, H_2O^- and H_3O. In the lower part of Tab. 1 (B) the formulae are given in apfu. In stilpnomelane K is predominantly replaced by Ba and subordinate by Na and Ca. BaO ranges between 1.63 to 3.36 wt. % and has on average of 23 analyses 2.53 wt. %. The respective data of the other oxides are: K_2O 0.45 to 1.62 (0.90); Na_2O 0.00 to 0.53 (0.15); and CaO 0.00 to 0.67 (0.22).

Chamosite: In contrast to stilpnomelane, chlorite is a rare mineral. Therefore, only 12 analyses (of three samples) could be carried out (Tab. 2). These analyses are presented in Fig. 17 occupying a small area within the field of chamosite with Si_{apfu} close to 2.9 and Fe/(Fe + Mg) about 7.5. A distinct correlation occurs between Fe and Mg the range of which lies between 33.79 and 37.87 (FeO) and 5.98 and 8.11 (MgO; Tab. 2, A).

Berthierine: Berthierine is similar in distribution and abundance as chamosite. It was detected in three samples only. Eleven analyses are presented in Tab. 3. In comparison with chamosite the FeO_{anal} and SiO_2 contents are higher and those of Al_2O_3 and MgO are lower. In Fig. 17 the analyses of Tab. 3 are plotted showing a larger compositional range than chamosite with Si_{apfu} varying from 3.0 to 3.5 and Fe/(Fe + Mg) ranging between 0.80 and 1.0.

Odinite: This mineral occurs in nearly every specimen. In Tab. 4 the analytical data including the calculated values of FeO, Fe_2O_3 and H_2O are summarized under A (wt. %). Under B the calculated values are presented (in apfu) resulting in the general formula of $(Fe^{2+},Mg,Al)_5[(OH)_6/(Si,Al)_4O_{10}]$. In Fig. 17 the analytical data of odinite (totally 13 analyses) occupy a relatively small area with $Si_{apfu} > 3.5$ and Fe/(Fe + Mg) close to 1.0.

CARBONATES

The chemical compositions of selected carbonates (31 representative analyses from about 300) are summarized in the Tabs. 5, 6 and 7. The carbonates belong either to the calcite group and their compositions represent calcite (Tab. 5, 11 analyses), siderite (Tab. 6, 10 analyses) and rhodochrosite (Tab. 7, 6 analyses) endmembers or belong to the dolomite group represented by dolomite and ankerite (Tab. 7, 4 analyses). The carbonate endmembers rhodochrosite, siderite, calcite, dolomite (arrowed from the left side) and ankerite (arrowed from the right side) are summarized in Fig. 18 which is the $MnCO_3$ - $FeCO_3$ - $CaCO_3$ diagram.

Calcite with CaO lying in the range between 46.59 and 53.04 wt. % is presented in Tab. 5. Six analyses have low MnO concentrations (0.04 - 0.49 wt. %; of columns I – VI), but relatively high FeO (2.20 – 6.34 wt. %) and SrO (0.65 – 1.76 wt. %) whereas five analyses reveal relatively high concentrations of MnO (2.57 – 7.81 wt. %; columns VII- XI) and slightly lower FeO (0.75 – 4.39 wt. %). Strontium, not occurring in the other carbonates, is a characteristic constituent of calcite (especially of the Mn-rich samples). The MgO concentrations of calcite are always relatively low (0.22 – 0.72 wt. %).

Siderite (Tab. 6) shows a wide range of the FeO, MgO, MnO and CaO concentrations (FeO: 30.94 - 58.90 wt. %; MnO: 0.04 – 22.49 wt. %; MgO: 0.27 – 9.34 wt. %; CaO: 0.08 – 9.54 wt. %).

Rhodochrosite is restricted to local enrichments and forms recrystallized masses representing originally collomorphic precipitation and is often zoned with siderite-rich centres and rhodochrosite-rich rims. Rhodochrosite has distinctly lower CaO (0.25 – 1.65 wt. %, exceptionally 6.12 wt. %, Tab. 7, column I) and MgO concentrations (0.09 – 1.00 wt. %) than siderite. MnO lies in the range between 43.55 and 61.17 wt. % [the latter value is identical with nearly pure rhodochrosite (column VI)]. The FeO-content ranges between 0.00 (column VI) and 13.73 wt. %.

The carbonates which belong to the dolomite group are presented in Tab. 7, columns VII – X. The concentrations of CaO are relatively constant (26.75 – 30.34 wt. %) whereas those of MgO, FeO and MnO show strong variations.

MAGNETITE

Six microprobe analyses of magnetite were carried out (Tab. 8). Apart from Si and Al (the latter in exceptions), the concentrations of Ti, Cr, V, Ni, Mn, Zn and Ca are very low. The Si-endmember which was verified by Newberry et al. (1982) and Ohkawa et al. (2007) by the substitution of $Si^{4+} \rightarrow Fe^{3+}$ reaches up to 2.75 wt. % (=10.4 mol. % of the theoretical endmember $Fe^{2+}_2SiO_4$) (Tab. 8, column I). The substitutions of $Al^{3+} \rightarrow Fe^{3+}$ leads up to 0.71 wt. % (=1.6 mol. % of the Al-member hercynite $Fe^{2+}Al_2O_4$) (Tab. 8, column II). The end-member concentrations of Mn, Mg, Ca, Zn, Ti, Cr and V do not exceed 0.15 wt. % (= 0.60 mol. %) (Tab. 8).

Four calculated formulae (wt. % data are not published) of different samples and later-mentioned magnetite types (see under discussion) are given below:

BL-41 (euhedral crystal): $[(Fe^{3+}_{0,024} Fe^{2+}_{0,975} Zn_{0,001})_{\Sigma=1,000} (Fe^{3+}_{1,925} Si_{0,075})_{\Sigma=2,000}]_{\Sigma=3,000}$ $O_{4,000}$; BL-60 (rice-grain shaped pseudomorph): $[(Fe^{3+}_{0,006} Fe^{2+}_{0,989} Ca_{0,002} Zn_{0,003})_{\Sigma=1,000}$ $(Fe^{3+}_{1,972} Si_{0,026} Al_{0,002})_{\Sigma=2,000}]_{\Sigma=3,000} O_{4,000}$;

BL-712 (porous crystal): $[(Fe^{3+}_{0,029} Fe^{2+}_{0,962} Mn_{0,001} Mg_{0,005} Ca_{0,001} Zn_{0,002})_{\Sigma=1,000}$ $(Fe^{3+}_{0,893} Si_{0,103} Al_{0,004})_{\Sigma=2,000}]_{\Sigma=3,000} O_{4,000}$;

L-1 (globular): $[(Fe^{3+}_{0,035} Fe^{2+}_{0,949} Mn_{0,010} Mg_{0,006})_{\Sigma=1,000} (Fe^{3+}_{1,862} Si_{0,129} Al_{0,009})_{\Sigma=2,000}]_{\Sigma=3,000} O_{4,000}$.

The contents of selected refractory trace elements in magnetite seperates are illustrated in Fig. 1. The contents of Ni are significantly higher than those of Co (median Ni = 35 ppm, Co = 6 ppm). Similarly, Ti is higher than V (median Ti = 273 ppm, V = 152 ppm). Co correlates well with Ni ($R^2 \sim 0.80$). The Ni/Co ratios lying around 5.8 are consistent with a low intensity of metamorphic transformation of the ores. The concentration of chromium is low (median = 30 ppm). A comparison of magnetite chemistry with an average tholeiitic basalt (Wedepohl 1975) indicates a broad agreement with the exception of Ti which is depleted (Fig. 20). However, this behaviour is typical for iron deposits in the Jeseníky Mountains.
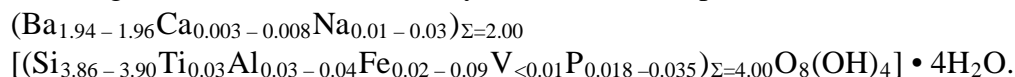
SULPHIDES

Among the sulphides, pyrite is the most abundant mineral which occurs in nearly all samples. Apart from elevated As (up to 0.17 wt. %) no other trace elements were detected by electron microprobe. However, quantitative spectral analyses showed <30 to 59 ppm Co, 25 to 640 ppm Ni (median 180 ppm), 2 to 300 ppm Ag (median 7 ppm), and <25 to 140 ppm V (Fig. 21). Arsenopyrite was detected in samples of the locality "BL". Apart from Ni (0.15 wt. %) other trace elements were not found.

The sulphides of Tab. 9 are exclusively from sample HB-906. Sphalerite (columns V and VII) shows relatively high Fe concentrations (about 7 wt. % equal to 0.12 apfu). Other elements detected are low: Mn, Ag, Co, Hg and As (lying between 0.05 and 0.19 wt. %). The

other two sulphides are <u>cobaltite</u> (Tab. 9, columns I – III) and a mineral of the <u>linneite</u> group (column IV).

KRAUSKOPFITE

Krauskopfite with the ideal formula of $Ba_2[Si_4O_8(OH)_4] \bullet 4H_2O$ (Strunz and Nickel, 2001) is a rare mineral (Fig. 15). The composition of krauskopfite is characterized by the presence of several trace elements (Ca, Na, Ti, Al, Fe, V, and P). Apart from Ca and Na, these elements can only be incorporated into the Si-position of the lattice of krauskopfite which has the following inferred formula (the analytical data are not published):

$(Ba_{1.94 - 1.96}Ca_{0.003 - 0.008}Na_{0.01 - 0.03})_{\Sigma=2.00}$

$[(Si_{3.86 - 3.90}Ti_{0.03}Al_{0.03 - 0.04}Fe_{0.02 - 0.09}V_{<0.01}P_{0.018 - 0.035})_{\Sigma=4.00}O_8(OH)_4] \bullet 4H_2O.$

SCHEELITE

This mineral is an accessory mineral in a few samples from the site "BL" (Reif 2000b, Reif and Vávra 2000). The scheelite grains are up to 0,0X mm in size and form intergrowths with stilpnomelane and corroded magnetite. The EDX analyses showed elevated contents of iron, which, however, may be caused by admixed magnetite.

Ore types and their whole-rock analyses

The iron ores that contain varying contents of opaque minerals (magnetite and pyrite), Fe-silicates and carbonates, are variable in textures and distributed irregularly to chaotically in the studied objects. The ores can be divided into three types which contain:

i) relatively high amounts of magnetite and subordinate Fe-silicates and carbonates (type I). The iron ores belong to the site "BL" shown in Fig. 3. The textures of these rocks are inhomogeneous, sometimes showing indications of schistosity. Magnetite, enclosed in a groundmass of carbonates (mainly siderite and calcite) and/or Fe-silicates, forms irregularly alternating clusters of isometric grains, fine-grained aggregates and rice-grain shaped crystals. Magnetite is frequently accompanied by pyrite, either disseminated or in massive aggregates representing up to 50 vol. % (type III). Clusters of quartz and finely dispersed hematite are relatively rare.

ii) high concentrations of Fe-silicates and carbonates (rhodochrosite, siderite and calcite) and low magnetite (type II). The rocks originate from the sites 2 and 3 („L" and HB-906 and HB-924 boreholes) of Fig. 4. Characteristic textures of these rocks are represented by concentric, initially most probably collomorphic aggregates (consisting of carbonate or silicate) and globular to hypidiomorphic diffusively zoned aggregates of Mn-Fe carbonate. Relics of fossils are also frequent.

13 whole-rock analyses of the three ore types are presented in the Tabs. 10 and 11. The analytical sum is lower than 100 (apart from one exception), indicating that iron (expressed as FeO) is partially also trivalent (Fe^{3+} was not determined) and that the content of water was not analyzed, but is present. Tab. 10 contains ores with high magnetite concentrations (type I), whereas Tab. 11 contains the other two types, namely silicate-rich (columns I – V, type II) and a pyrite-rich ore (column VI, type III). The three types differ distinctly in their concentrations of FeO, CO_2, CaO, SiO_2, but in particular in that of MnO. Whereas in the magnetite-rich ores (Tab. 10) the MnO concentration is relatively constant and low (varying between 0.26 and 0.93 wt. %), in the silicate-rich ores the MnO contents vary in a wide range (0.13 and 19.05 wt. %, Tab. 11).
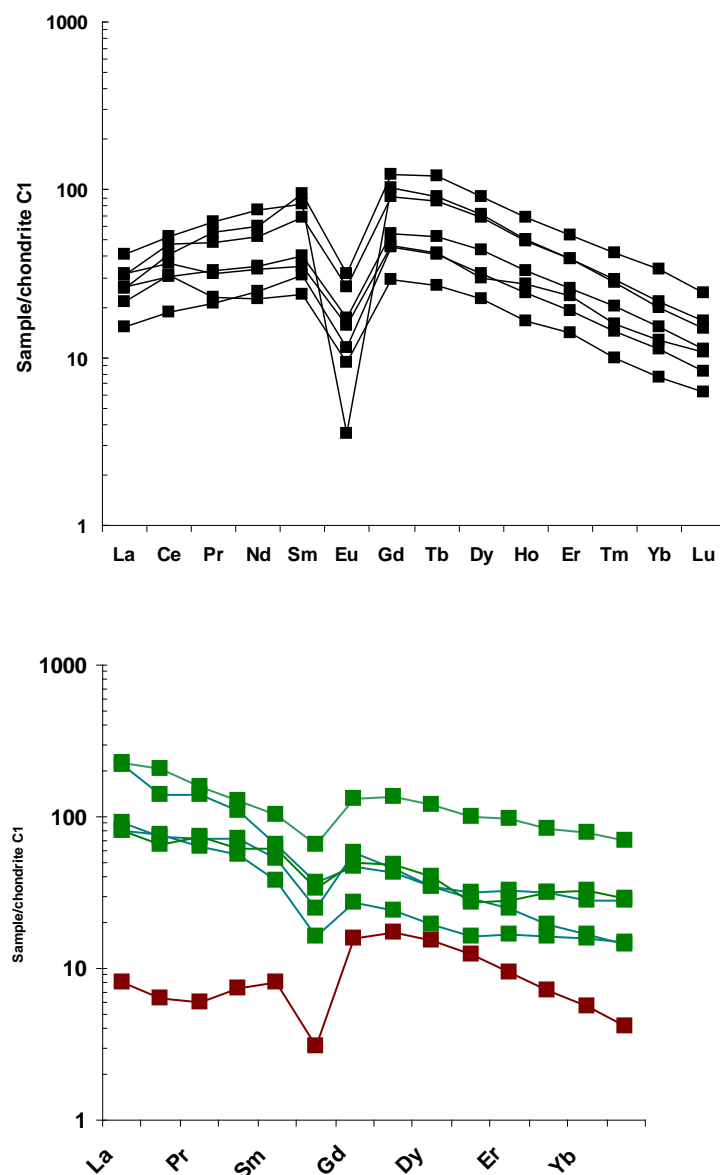
Fig 22: Chondrite-normalized REE patterns. Upper part: magnetite-rich ore (black). Bottom part: silicate-rich ore (green) and pyrite-rich ore (brown) of the ore bodies.

REE analyses

In total 13 analyses were carried out. Tab. 12a contains the magnetite-rich ore (type I), whereas Tab. 12b those with low contents of magnetite and high contents of the Fe-silicates (ore type II; columns I - VI) and a pyrite-rich one (ore type III; column VII). In general, the REE contents are very low, especially in type III (Σ_{REE}= 21.66 ppm) and type I (Σ_{REE}= 56.93 – 149.33 ppm). In relation to these two ranges that of ore type II is slightly higher (Σ_{REE}= 120.75 – 304.25 ppm). The ΣHREE/ΣLREE ratios are between 1.13 and 2.36 (ore type I) and 2.74 and 6.58 (ore type II). The corresponding value for ore type III is the lowest (1.01).

The C1-chondrite normalized REE patterns (Anders, Grevesse 1989) are different for mineralogically distinct types of ore: the magnetite ore show a MREE-enrichment, whereas the silicate-rich ores show patterns typical for differentiated tholeiitic rocks (Fig. 22). In agreement with these findings are also the different Eu and Ce anomalies calculated according to McLennan (1989). The Eu anomaly of the magnetite ores has a value lying in the range of

0,039 – 0,388, whereas that of the Fe-silicate ores lies between 0,450 and 0,659. For the Ce anomalies the following values were detected for the magnetite ores: 1,01 – 1,40; and for Fe-silicate ores: 0,81 – 1,09.
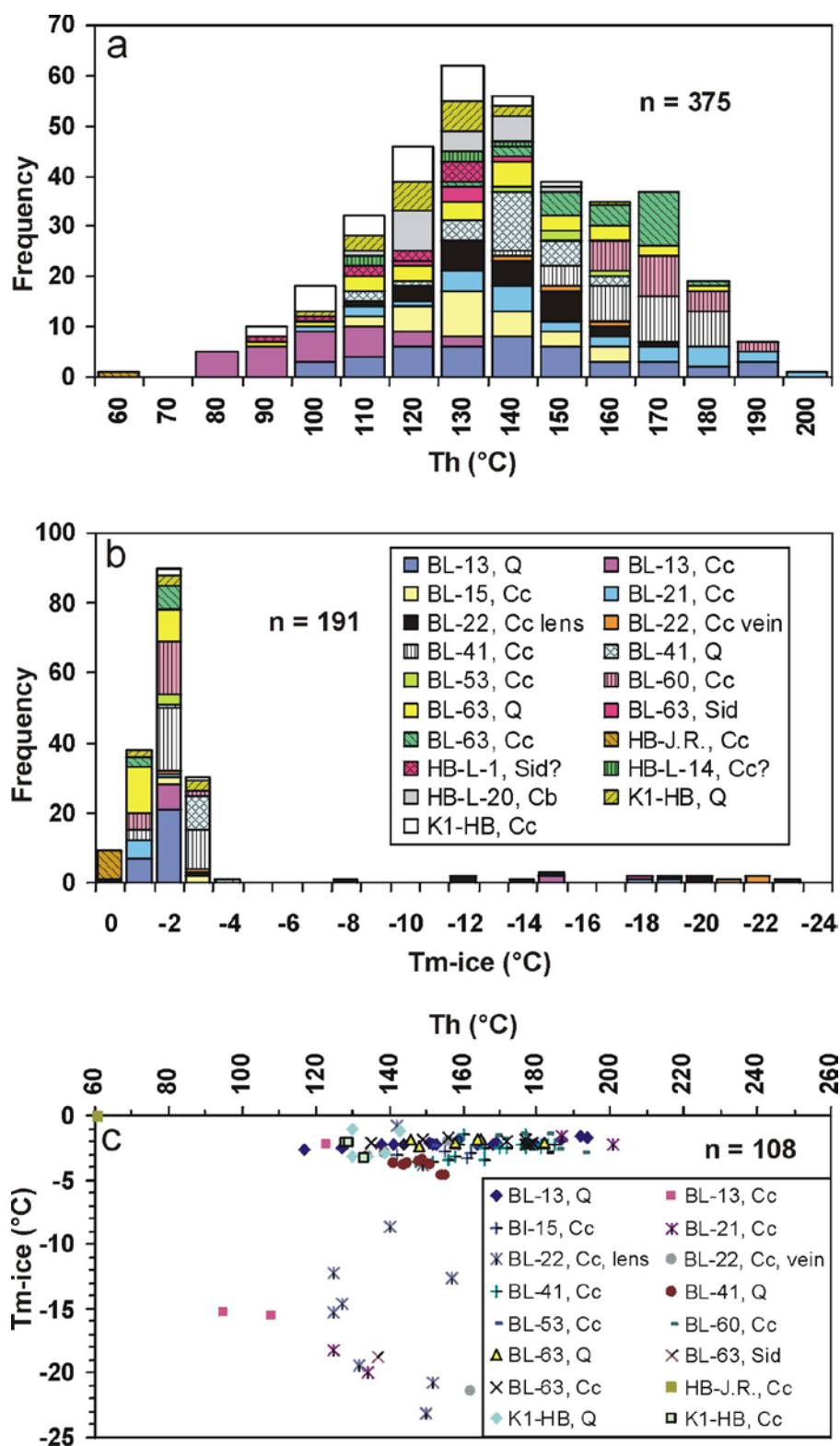
Fig 23: A graphical presentation of the results of the fluid inclusion microthermometry. **a -** histogram of homogenization temperatures of two-phase (L+V) inclusions; **b -** histogram of melting temperatures of last crystal of ice; **c -** Th-Tm plot.

Fluid inclusions

Fluid inclusions were studied in carbonates (calcite, siderite, rhodochrosite) and quartz which have been sampled from both ore matrix and veins. A significant similarity in petrographic characteristics can be stated when the genetically different samples are compared.

Abundant primary fluid inclusions in the calcite and quartz samples often have a regular three-dimensional distribution, or occur in clusters, growth zones, or as solitary inclusions. The pseudo-secondary inclusions mostly occur along short non-continuous cracks. In most of the samples from both vein and rock matrix usually host not only one-phase (L) but also two-phase (L+V) fluid inclusions in various proportions in individual samples. The L-inclusions often exhibit smaller sizes in comparison with L+V inclusions, pointing to probable metastability of their phase composition. The L+V inclusions mostly display constant water volume fractions (ca. 90–95). The P and PS inclusions have negative-crystal, isometric, oval or irregular shape void of any tips and mostly reach 5–10 μm in size. The secondary inclusions occurring in trails cutting the whole grain are mostly all-liquid (L), less frequently L+V.

The homogenization temperatures of two-phase P and PS L+V inclusions show rather wide range between 85 and 218 °C, however, a narrower variability is usually observed for individual samples (Tab. 13, Fig. 23). There is no significant difference between Th values of rock- and vein-hosted fluid inclusions (Fig. 23). The homogenization of scarce L+V inclusion from sample of the calcite crystal from the drusy vug revealed lowest Th value of 61 °C, compatible with the presence of prevailing L-inclusions in this sample, which is indicative for very low formation temperatures not exceeding ca. 50 °C (Reynolds & Goldstein 1990) .

The fluid inclusions freeze at temperatures between –40 and –47 °C in a majority of samples, remaining colorless. The phase transitions other then final melting of ice (occurring between –0.8 and –3.8 °C) and rarely observed eutectic melting (between –35 and –39 °C) are invisible in these inclusions. Many inclusions behave metastable during freezing due to elimination of the vapor phase during ice formation. A part of inclusions hosted by samples BL-13, BL-21, BL-22 and BL-63 displayed a granular texture, dark brown coloration of frozen inclusion content and much lower Tf, Te and Tm-ice values (down to –85 °C, –56 °C, and –23.2 °C, respectively; Tab. 13, Fig. 23). There are no systematic differences between coexisting inclusions differing in phase composition (L, L+V). A calcite crystal from drusy vug showed the uppermost observed Tf and Tm-ice values of the whole dataset (–29 to –39 °C and –0.1 to 0.0 °C, respectively).

Stable isotopes

Carbon and oxygen isotope compositions have been determined in four rhodochrosite, siderite and calcite samples. The $\delta^{18}O$ values of rhodochrosite and siderite show a narrow range between 23.3 and 23.9 ‰ SMOW, whereas the variability of their $\delta^{13}C$ values is somewhat greater, between –10.2 and –16.3 ‰ PDB. The new carbon and oxygen isotope data of Fe-Mn carbonates less or more overlap with range reported by Reif (2000b), who found $\delta^{13}C$ = -14.0 to -27.1 ‰ PDB and $\delta^{18}O$ = 22.4 to 23.4 ‰ SMOW (n = 3). By contrast, the calcite from drusy vug had $\delta^{13}C$ value of -11.8 ‰ PDB and $\delta^{18}O$ value as low as 18.5 ‰ SMOW.

Sixteen magnetite separates were analyzed for $\delta^{18}O$ values. The data range between 2.5 and 10.4 ‰ SMOW (Fig. 24). The limestone-hosted magnetites show markedly elevated $\delta^{18}O$ values (8.3 to 10.4 ‰ SMOW then samples from other settings (2.5 to 6.7 ‰ SMOW).

The $\delta^{34}S$ values were determined in twenty-nine pyrite samples taken from both iron ore matrix and younger veins. The $\delta^{34}S$ values of pyrites from iron ore matrix range between -2.9

and +20.4 ‰ CDT with most data being highly positive between +16 and +20 ‰ CDT (Fig. 24). Three pyrite samples from crosscutting veins have $\delta^{34}S$ values between +18.6 and +20.4 ‰ CDT being identical with the majority of pyrites sampled from ore matrix (Fig. 24). The $\delta^{34}S$ data of pyrites from iron ore are different from those of pyrites sampled from basic volcanites in the wider surrounding, which show most analyses tightly clustering around 0 ‰ CDT (+0.0 to +0.9 ‰ CDT; n = 6; Fig. 24).
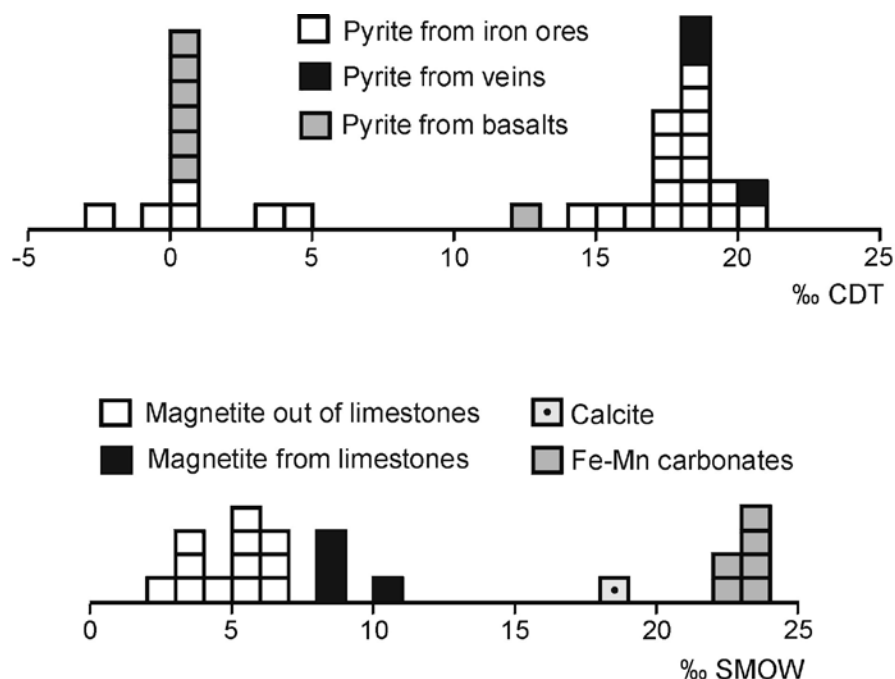
Fig 24: A comparison of $\delta^{34}S$ values of pyrites sampled from iron ores and those from veins hosted by iron ores with pyrites from basic volcanites (up), and variations in $\delta^{18}O$ values of magnetites and carbonates from iron ores (bottom).
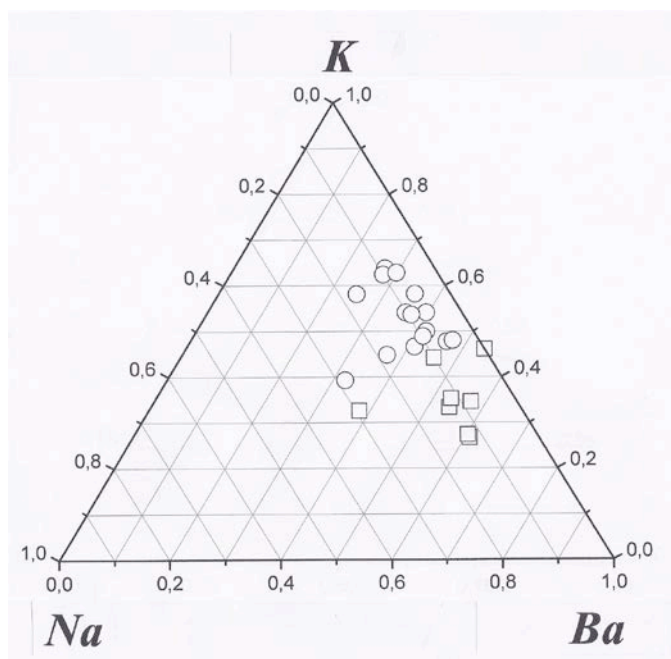
Fig 25: Ba-K-Ca diagram in apfu and the analytical plots of stilpnomelane (circle) and eight plots showing Ba-stilpnomelane (quadrangle).
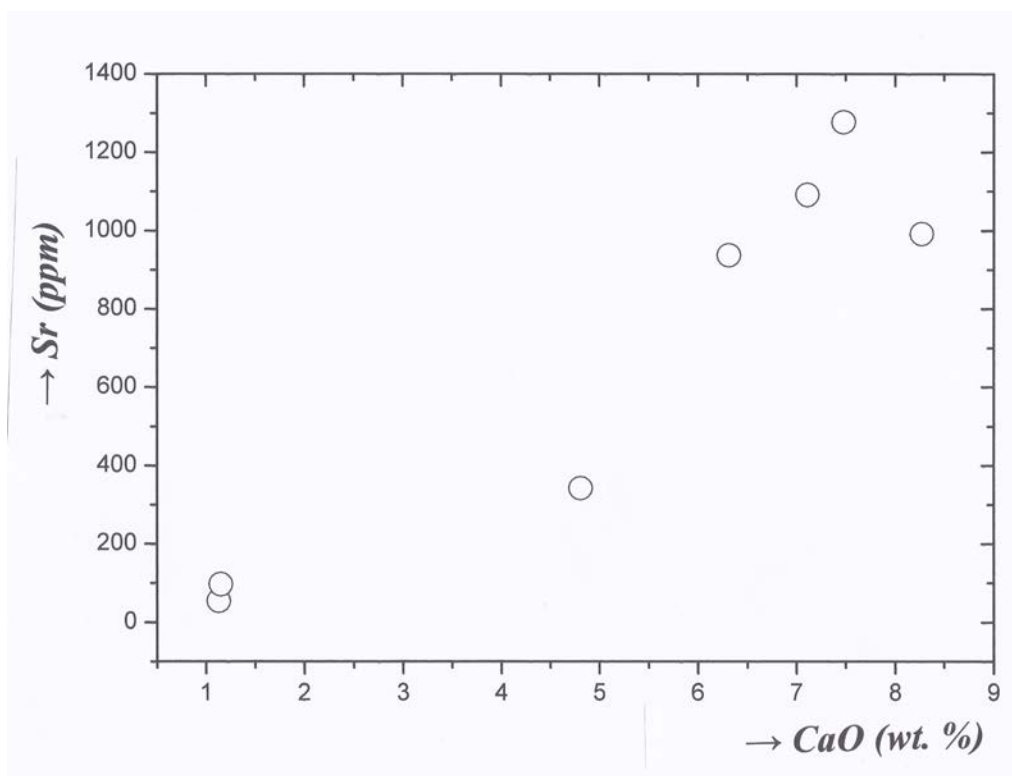
Fig 26: Sr (ppm) – CaO (wt. %) diagram and the analytical plots of magnetite-rich ores (Tab. 10).
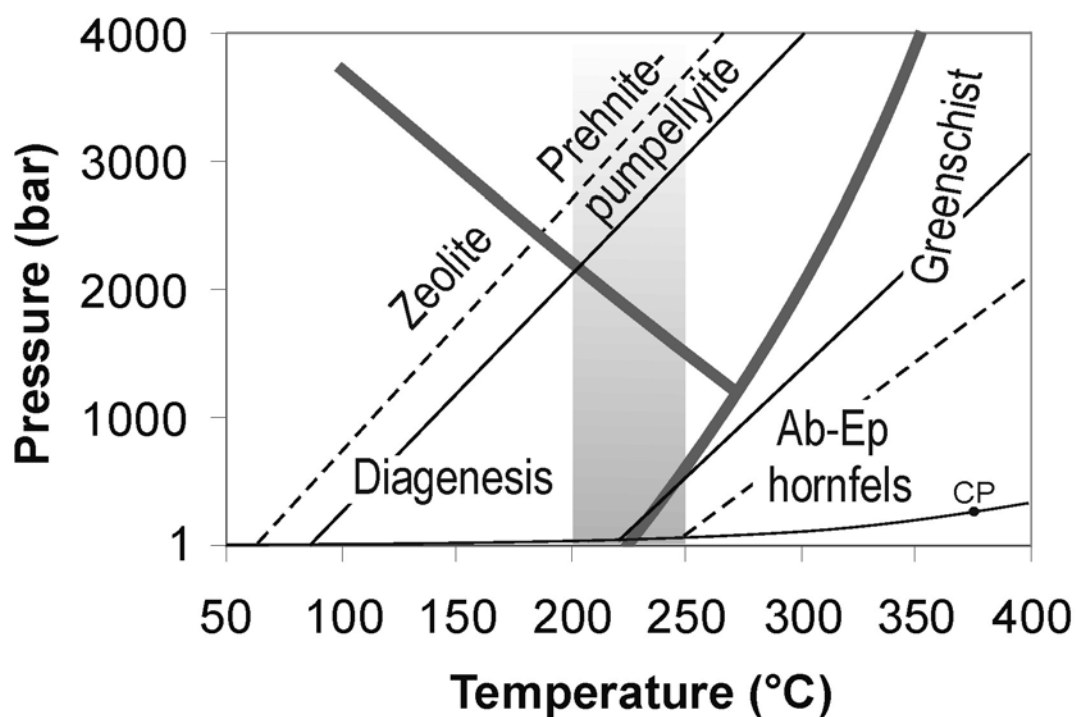
Fig 27: Position of isochores of fluid inclusions from the studied iron ores (full lines) in the PT-space. The grey field indicates maximum temperatures of metamorphic overprint indicated by earlier studies of organic matter (Kříbek 1977, Müller 1981). Petrogenetic grid was taken from Krauskopf and Bird (1995). CP critical point for pure water. Isochores of fluid inclusions from sulphide Zn-Pb-Ba deposit at Horní Benešov (Fojt et al. 2010) are visualized by dashed lines.

Tab 9: Selected analyses of colbaltite, linneite, and sphalerite (wt. %; A) and calculated atoms per formula unit (apfu; B).

	Cobaltite			Linneite	Sphalerite		
				HB – 906			
	I	II	III	IV	V	VI	VII
A: Weight-percent (wt. %)							
Fe	6.64	5.33	6.15	19.07	7.04	7.04	6.77
Mn	-	0.04	0.06	0.06	-	-	0.19
Co	22.75	28.18	26.50	13.55	0.04	0.04	
Ni	7.57	4.48	4.95	1.92	-	-	
Cu	-	-	0.04	20.40	-	-	
Ag	-	0.07	-	0.04	-	0.08	0.03
Zn	-	-	-	-	60.14	60.23	60.02
Hg	-	-	-	-	-	0.05	-
Cd	-	-	0.04	0.03	0.05	-	0.05
S	19.27	22.31	21.42	33.81	32.70	32.97	33.57
As	44.70	40.37	41.48	10.76	-	0.08	0.12
Sb	0.05	0.14	-	-	-	-	-
Σ	**100.98**	**100.92**	**100.64**	**99.64**	**99.83**	**100.49**	**100.83**
B: Atoms per formula unit (apfu)							
Fe	0.195	0.152	0.177	1.125	0.122	0.121	0.116
Mn	-	0.001	0.002	0.004	-	-	-
Co	0.632	0.760	0.722	0.757	-	0.001	-
Ni	0.211	0.121	0.135	0.108	-	-	-
Cu	-	-	0.001	1.057	-	-	-
Ag	-	0.001	-	0.001	-	-	-
Zn	-	-	-	-	0.890	0.886	0.878
Hg	-	-	-	-	-	0.001	-
Cd	-	-	0.001	0.001	-	-	-
Σ	*1.038*	*1.035*	*1.038*	*3.057*	*1.012*	*1.009*	*0.997*
S	0.985	1.106	1.073	3.470	0.988	0.990	1.001
As	0.976	0.857	0.889	0.473	-	0.001	0.002
Sb	0.001	0.002	-	-	-	-	-
Σ	*1.962*	*1.965*	*1.962*	*3.943*	*0.988*	*0.991*	*1.003*

Tab 10: Whole-rock composition of magnetite-rich ores of the ore body (wt. % in A, ppm in B).

	Magnetite-rich rocks						
	I	**II**	**III**	**IV**	**V**	**VI**	**VII**
	HB-BL 13	**HB-BL 41**	**HB-BL 54**	**HB-BL 56**	**HB-BL 60**	**HB-BL60a**	**HB-BL62**
A: Weight-percent (wt. %)							
SiO_2	5.89	15.75	7.51	8.89	17.73	15.36	13.60
TiO_2	<0.01	<0.01	0.04	0.05	<0.01	<0.01	0.10
Al_2O_3	0.61	0.20	0.71	1.00	0.26	0.20	1.55
FeO	71.25	56.71	62.62	60.42	58.01	61.77	54.40
Cr_2O_3	<0.002	<0.002	<0.002	0.003	<0.002	<0.002	<0.002
P_2O_5	0.04	0.02	0.02	0.07	<0.01	0.05	0.01
MgO	0.77	0.35	0.91	1.63	0.47	0.25	1.67
CaO	4.81	8.27	7.48	1.13	6.31	7.11	1.15
MnO	0.93	0.63	0.26	0.89	0.36	0.82	0.45
Na_2O	0.03	<0.01	0.03	0.05	0.01	<0.01	0.03
K_2O	0.14	0.04	0.16	0.23	0.06	0.06	0.20
CO_2	10.21	14.05	15.66	22.40	12.92	11.05	21.76
S	0.27	0.11	0.41	0.41	0.29	0.85	1.73
Σ	**94.95**	**96.11**	**95.81**	**97.17**	**96.48**	**97.52**	**96.65**
B: Parts per million (ppm)							
Mo	26	39	24	11	46	68	n.d.
Cu	6	1	28	9	2	8	11
Pb	260	416	678	185	483	340	256
Zn	2342	1282	2011	1274	1916	1245	1864
Ni	10	9	24	70	14	124	36
As	205	28	115	29	41	236	427
Cd	0.2	0.1	0.7	0.1	0.3	0.2	0.2
Sb	8	8	9	10	10	18	5
Ag	0.2	0.8	1	0.4	0.2	0.3	1
Au_{ppb}	3	5	1	15	2	1	3
Hg	n. a.	0.04	<0.01	0.04	0.06	<0.01	<0.01
Se	0.6	0.6	2	<0.5	<0.5	1	0.6
Sc	1	21	2	1	1	<0.1	3
Ba	2748	522	3488	4307	2574	1941	3342
Be	21	4	28	31	175	75	16
Co	1.2	8	1.4	0.8	1	0.7	2
Cs	10	14	9	13	2	2	13
Ga	15	24	14	8	7	7	18
Hf	0.2	<0.1	0.2	0.4	0.1	<0.1	0.8
Nb	9	0.5	2	2	3	1	5
Rb	6	2	5	10	2	2	8
Sr	342	992	1277	55	937	1091	97
Th	0.3	<0.2	1.1	0.9	<0.2	<0.2	2
U	1.3	0.8	0.9	0.8	2	1.2	1.3
V	122	108	153	45	54	25	36
W	792	165	705	52	138	188	509
Zr	13	2	17	14	6	2	32
Y	91	37	53	49	74	83	27

Tab 11: Whole-rock composition of silicate- and pyrite-rich ores of the ore body (wt. % in A, ppm in B).

	Silicate-rich rocks					*S-rich*
	I	**II**	**III**	**IV**	**V**	**VI**
	Hb-BL48	**HB-BL 58**	**HB-906**	**HB-L 16**	**HB – L 14**	**HB-M7 PY**
A: Weight-percent (wt. %)						
SiO_2	7.58	22.10	17.50	10.13	9.43	15.99
TiO_2	0.06	0.13	0.23	0.04	0.04	0.01
Al_2O_3	1.33	5.64	5.29	3.88	3.36	0.90
FeO	49.20	25.38	48.90	38.68	53.53	47.30
Cr_2O_3	0.002	0.002	0.007	0.003	<0.002	<0.002
P_2O_5	0.11	0.05	0.39	0.08	0.09	0.01
MgO	1.27	3.09	2.77	1.92	0.44	0.89
CaO	15.12	0.77	3.14	0.76	0.59	0.59
MnO	0.64	19.05	0.13	15.29	9.95	0.22
Na_2O	0.01	0.09	0.18	0.03	0.02	0.04
K_2O	0.07	0.21	0.29	0.11	0.07	0.16
CO_2	21.36	18.56	15.15	23.79	18.96	0.51
S	0.32	2.19	0.18	5.86	0.73	36.97
Σ	*97.07*	*97.26*	*94.15*	*100.17*	*97.21*	*100.73*
B: Parts per million (ppm)						
Mo	16	64	5	50	38	38
Cu	93	63	28	93	13	119
Pb	136	399	42	193	268	114
Zn	642	709	81	1421	1943	2455
Ni	14	32	134	93	41	8
As	162	120	14	6040	1275	793
Cd	<0.1	0.7	<0.1	3	1.2	1
Sb	3	10	1	30	42.9	10
Ag	0.2	5	<0.1	6	0.2	24
Au_{ppb}	0.6	<0.5	20	0.7	10	1.3
Hg	n.a.	0.2	0.04	0.2	<0.01	0.3
Se	<0.5	<0.5	<0.5	3	0.6	1
Sc	4	5	7	4	6	2
Ba	820	6123	258	3189	1780	5558
Be	112	3	3	5	33	57
Co	4	3	26	4	0.4	0.3
Cs	5	10	39	5	6	9
Ga	4	23	13	27	18	5
Hf	0.5	2	2	0.5	0.4	0.3
Nb	1.5	7	6	2	1.3	1.3
Rb	3	7	10	4	3	7
Sr	204	31	66	23	22	92
Th	0.8	6	4	1.4	0.6	0.4
U	0.3	1.5	2.5	2	2	0.3
V	62	95	251	135	289	38
W	352	19	6	102	821	8
Zr	18	65	67	21	24	10
Y	55	83	24	145	31	18

Tab 12a: REE contents of the magnetite-rich ores (ppm).

	I	II	III	IV	V	VI	VI
	HB-Bl-13	*HB-BL-41*	*HB-BL-54*	*HB-BL-56*	*HB-BL-60*	*HB-Bl-60a*	*HB-BL-62*
La	6.1	3.6	6.2	7.5	7.3	9.7	5.0
Ce	25.0	11.3	18.2	21.9	28.7	31.4	18.7
Pr	4.93	1.88	2.93	2.81	4.35	5.76	2.04
Nd	27.6	11.3	15.8	15.2	23.9	34.0	10.2
Sm	13.80	4.56	5.98	5.11	10.10	12.00	3.53
Eu	1.76	0.64	0.96	0.87	1.48	1.71	0.52
Gd	24.29	8.95	10.74	9.19	18.01	20.23	5.78
Tb	4.35	1.47	1.9	1.51	3.07	3.25	0.98
Dy	22.08	7.68	10.67	7.21	16.70	17.47	5.40
Ho	3.84	1.36	1.85	1.53	2.76	2.84	0.92
Er	8.55	3.01	4.08	3.73	6.12	6.14	2.23
Tm	1.01	0.34	0.49	0.38	0.67	0.70	0.24
Yb	5.44	1.00	2.5	2.08	3.23	3.47	1.24
Lu	0.58	0.20	0.27	0.26	0.36	0.40	0.15
ΣREE	149.33	58.13	82.57	79.26	126.75	149.07	56.93
ΣHREE	79.19	33.29	50.07	53.39	75.83	94.57	39.99
ΣLREE	70.14	24.85	32.50	25.87	50.92	54.50	16.94
ΣH/ΣL	1.13	1.34	1.54	2.06	1.49	1.74	2.36

Tab 12b: REE contents of the silicate- and pyrite-rich ores (ppm).

	I	II	III	IV	V	VI	VI
	HB-Bl-48	*HB-BL-58*	*HB-906*	*HB-L-6*	*HB-L-14*	*HB-L-15*	*HB-MT-Py*
La	21.5	59.2	19.2	53.5	19.2	52.0	1.9
Ce	45.1	107.7	46.2	122.2	39.7	85.3	3.8
Pr	6.45	13.21	5.68	14.13	6.56	12.36	0.53
Nd	32.5	54.5	25.4	57.0	27.6	49.9	3.3
Sm	7.77	12.04	5.64	16.01	8.97	9.64	1.18
Eu	1.39	2.29	0.92	3.65	1.86	2.05	0.17
Gd	11.42	15.87	5.31	26.18	9.73	9.26	3.11
Tb	1.47	2.79	0.86	4.84	1.72	1.53	0.62
Dy	8.60	15.58	4.72	20.05	9.75	8.31	3.69
Ho	1.61	3.24	0.90	5.53	1.52	1.76	0.70
Er	3.90	8.83	2.63	15.32	4.39	5.20	1.48
Tm	0.47	1.19	0.39	2.01	0.76	0.77	0.17
Yb	2.74	6.86	2.54	12.65	5.37	4.60	0.91
Lu	0.35	0.95	0.36	1.65	0.70	0.67	0.10
ΣREE	145.27	304.25	120.75	363.72	137.83	243.35	21.66
ΣHREE	114.71	248.94	103.04	266.49	103.89	211.25	10.88
ΣLREE	30.56	55.31	17.71	97.23	33.94	32.10	10.78
ΣH/ΣL	3.75	4.45	5.82	2.74	3.06	6.58	1.01

Tab 13: Results of microthermometric measurements of fluid inclusions. Temperature parameters are in °C, salinity in wt. % NaCl eq.

Sample	Description	Mineral	Genesis	Phase comp.	LVR	Th (L+V)	Tf	Te	Tm hh	Tm ice	Salinity	Salt system
BL-13	Stilpnomelane-bearing vein	Quartz	P, PS	L+V, L	0.9-1	104-194	-40/-44	-39		-1.6/-2.6	2.7-4.3	Mg-Na-Cl
			S?	L+V	0,9	94		-50		-6.9/-8.6	10.4-12.4	Ca-Na-Cl
		Calcite	P	L+V, ojed. L	0.9-1	85-134	-41/-61	-35/-48		-2.2/-15.5	3.7-19.0	Mg/Ca-Na-Cl
			S?	L+V	0,8	211-218	-75	-55	-24,8	-20.9/-21.1	23.0-23.1	Ca-Na-Cl
BL-15	Ore-forming, older, turbid	Calcite	P	L+V	0,9	117-164	-47			-2.9/-3.3	4.8-5.4	
	Ore-forming, younger, clear	Rhodochrosite?	P	L+V	0,9	155	-46			-2,8	4,6	
	Younger veinlets	Calcite	P	L+V, L	0.9-1	118						
			PS-S?	L+V	0,9	120-157						
BL-21		Calcite	P	L+V, L	0.9-1	109-201	-40/-85			-1.0/-19.9	1.7-22.3	
BL-22	Lens, older turbid	Calcite	P	L+V, L	0.9-1	137-171	-46			-0.8/-3.8	1.4-6.2	
	Lens, younger clear	Calcite	P	L+V, L	0.9-1	115-157	-67/-76	-50		-8.6/-23.2	12.4-24.5	Ca-Na-Cl
	Younger colourless vein	Calcite	P	L+V	0,9	143-162	-42/-75			-2.0/-22.5	3.4-24.0	
BL-41	Ore-forming	Quartz	P, PS	L+V	0,9	110-165	-42/-46			-2.9/-4.7	4.8-7.4	
	Ore-forming	Calcite	P, PS	L+V	0.9	147-187	-42/-46	-38		-1.5/-3.5	2.6-5.7	Mg-Na-Cl
BL-53	Younger vein	Calcite	P	L+V	0.9	147-161	-43/-44			-2.4/-2.5	4.0-4.2	
BL-63	Ore-forming	Quartz	P, PS	L+V, L	0.9-1	98-182	-39/-44	-38		-1.8/-2.4	3.1-4.0	Mg-Na-Cl
			S	L+V	0,9		-48	-48		-9,9	13,8	Ca-Na-Cl
	Older vein	Siderite	P	L, L+V	0.9-1	129-140	-68	-56		-18,8	21,5	Ca-Na-Cl
	Younger vein	Calcite	P	L+V, L	0.9-1	135-184	-42/-45			-1.7/-2.2	2.9-3.7	
BL-60	Ore-forming among magnetite crystals	Calcite	P	L+V	0.9	161-193	-44/-47			-1.4/-3.3	2.4-5.4	
HB-L-1	Youngest yellowish coarse-grained	Siderite?	P, PS	L, L+V	0.9-1	99-139	-46					
HB-L-14	Veinlet	Calcite?	P	L, ojed. L+V	0.9-1	118-146	-44					
HB-L-20	The oldest, turbid	Carbonate	P, PS	L, ojed. L+V	0.9-1	116-152	-44					
HB-906	Quartz- and stilpnomelane-bearing vein	Calcite	P, PS	L+V, L	0.9-1	125-151	-42/-46			-1.9/-3.3	3.2-5.4	
K1-HB	Vein	Calcite	P	L, L+V	0.9-1	98-154	-37/-45			-2.1/-3.3	3.5-5.4	
		Quartz	P	L+V, L	0.9-1	106-168	-44/-46			-1.0/-3.2	1.7-5.3	
J.R.	Crystal from a vein	Calcite	P	L, ojed. L+V	0.95-1	61	-29/-39			0.0/-0.1	0.0-0.2	

Discussion

Whole-rock analyses

Apart from some chemical similarities of rock-type I (magnetite-rich rocks; Tab. 10) and II (silicate-rich rocks, Tab. 11), the FeO-(MgO + CaO + MnO)-CO_2 clearly reveal strongly varying concentrations, especially of MnO. The high MnO contents of rock-type II correspond with high CO_2 concentrations (Tab. 11, columns II, IV, and V) indicating the presence of rhodochrosite. In the magnetite-rich types, the CO_2 concentrations may be of similar size (Tab. 10, columns IV, VII, and III), but correspond with the high Fe concentrations of siderite. Rock-type III (pyrite-rich) differs from the other two types due to its high S-content (36.97 wt. %) and thus, corresponding lower concentrations of the other elements.

The trace element concentrations confirm the well-known fact that the Fe-ore deposits of the Jeseníky area are notoriously low in titanium. The high concentrations of Pb (up to 678 ppm), Zn (up to 2455 ppm) and As (up to 6040 ppm) and low Cu (max. 119 ppm) agree with the observation that

arsenopyrite shows local enrichments and reveals that the disseminated sulphides are represented by sphalerite and galena rather than chalcopyrite. The occurrence of stilpnomelane, barite and krauskopfite seems to be connected with the occurrence of barium (up to 6123 ppm). In Tab. 10 (magnetite-rich type), the concentration of strontium (up to 1091 ppm) depends on that of CaO (as a component of calcite). The relatively elevated contents of tungsten (up to 821 ppm) can be explained with the presence of accessory scheelite in the ore body.

The negative Ce anomaly (Fig. 22) could indicate seawater as parent fluid (cf. Mc Lennan 1989) from which the protolith of iron ores precipitated, whereas the positive Ce anomaly could be related to remobilization of Ce from marine sediments. Alternatively, the rather non-systematic variability of Ce anomaly can simply reflect the changing oxygen fugacity in the parent fluid. The different REE distribution patterns for mineralogically distinct types of ore (Fig. 22) would indicate rather different initial composition of their protoliths (i.e., higher contents of volcanic material in silicate-dominating ores, higher amount of precipitations from the seawaters in magnetite-rich ores) than fractionation of REEs from a single source (i.e., submarine fluids).

Silicates

The first analysis of Ba-bearing <u>stilpnomelane</u> from Horní Benešov was published by Zimák (2004). In older analyses of this mineral from Horní Benešov and similar Fe-deposits of the Šternberk-Horní Benešov Belt Ba was not analyzed (Babčan 1958, Melka & Vybíral 1977, Zachař 1983, Reif 1985, Zimák 1999, Zimák & Vávra 1998, Zimák et al. 1998, Reif 2000a). However, in our stilpnomelane analyses K occurs together with Ba and subordinate Na and Ca (Tab. 1). Therefore, the general formula is $(K, Ba, Na, Ca, H_3O)_{1.00}(Fe^{2+}, Mg)_8[(OH)_8/(Si,Al)_{12}O_{28}] \cdot 2H_2O$. Apart from one exception (Tab. 1, column XI) the K_2O, Na_2O, CaO and BaO contents (in wt. %) reveal that in all samples BaO predominates over K_2O and that the latter is always higher than Na_2O as well as CaO (Tab. 1). Fig. 25 is the Ba-K-Na diagram (in mol. %) which shows that eight plots (quadrangle) represent Ba-dominated stilpnomelane. According to our knowledge, no other locality is known in the world revealing such high Ba-concentrations in stilpnomelane.

<u>Chamosite</u> yielded a temperature of formation lying in the range of 252 to 306 °C (286 °C on average, Cathelineau 1988). The temperatures derived by the equation by Jowett (1991) are slightly higher (266 to 319 °C; 300 °C on average; see Tab. 2, last two lines). For comparison, Fig. 17 contains chamosite from the Malý Děd iron occurrence (Mücke et al. 2010) showing slightly higher Fe/(Fe+Mg) ratios than those of Horní Benešov. It is well-known that increasing temperature of metamorphism led to a decrease of the Fe/(Fe+Mg) ratio. It is also well-known that the degree of metamorphism at Horní Benešov is distinctly lower than in Malý Děd. Therefore we conclude that the protolith of the ores at Horní Benešov was Mg-richer than that of Malý Děd. Differences of the Fe/Mg ratios in chlorites from both the Vrbno Group and the Šternberk-Horní Benešov Belt was also mentioned by Kopecká (2012).

<u>Berthierine</u> has the same formula as chlorite $(Fe,Mg,Al)_6[(OH)_8/AlSi_3O_{10}]$, but belongs to the serpentine group (Strunz and Nickel 2001). In comparison with chlorite, berthierine has distinctly higher FeO, slightly higher SiO_2 and distinctly lower Al_2O_3 (Tab. 3). These differences become recognizable in Fig. 17, where the field of berthierine differs clearly from that of chamosite which is relatively small. The existence of berthierine was confirmed by XRD investigations too. Berthierine was firstly discovered in massive sulphide deposits (Kidd Creek in Ontario, Canada) by Slack et al. (1992).

<u>Odinite</u> was originally thought to be greenalite, which is known in the Moravo-Silesian Lahn-Dill type deposits (e.g. Melka & Vybíral, 1977). Greenalite has the formula of $(Fe^{2+},Fe^{3+})_{>6}[(OH)_8/Si_4O_{10}]$ and belongs, like berthierine, to the serpentine group (Strunz and Nickel, 2001). However, our analyses (Tab. 4) contain always Al_2O_3 (up to 14.58 wt. %, column X) and MgO (up to 6.28 wt. %, column X) indicating that the mineral is not identical with greenalite, but with odinite which has the formula of $(Fe^{2+},Mg,Al)_5[(OH)_8/(Si,Al)_4O_{10}]$ (Strunz and Nickel, 2001). Calculating the results of our analyses with this formula, the data show that nearly all the analyzed iron has to be trivalent. This contradicts the observation that the colour of the mineral is distinctly green indicating the predominance of divalent iron. At the same time the calculated data show an analytical total which is always higher than 100 wt. % (up to 105 wt. %). The only formula which fits well to our results has

lower OH-content and the following inferred formula of $(Fe^{2+},Mg,Al)_5[(OH)_6/(Si,Al)_4O_{10}]$. Calculations based on this formula (with lower H_2O content and with iron predominantly in the divalent oxidation state) reduced the analytical sum always close to 100 wt. % (Tab. 4).

In Fig. 17, the analytical plots of odinite are presented indicating that the composition is relatively constant with high Fe and Si concentrations in relation to chamosite and berthierine. Odinite which seems to be extensively a rare mineral occurs in diagenetic to low grade metamorphic marine sediments and may be associated with berthierine (e.g. Hornibrook & Longstaffe 1996).

Carbonates

Calcite occurs in two types. Calcite from ore type I has low rhodochrosite concentrations (0.06–0.70 mol. %), but relatively high siderite (3.09 - 8.94 mol. %). The strontianite content lies in the range between 0.64 and 1.72 mol. %. Calcite from ore type II has higher concentrations of $MnCO_3$ (3.61–11.31 mol. %), lower $FeCO_3$ (1.05–6.19 mol. %) and on average lower $SrCO_3$. These two types can also be easily differentiated by observations under the microscope. The first is coarse-grained and has nearly always corroded grain boundaries (Fig. 9) and represents obviously clastic material (diameter up to 400 μm) that may contain inclusions of stilpnomelane (Fig. 10). The second is often associated with siderite in the form of recrystallized former collomorphic masses (Fig. 11).

The calcite chemistry is visualized in Fig. 18 ($MnCO_3 – FeCO_3 – CaCO_3$ diagram). The plots (33 circles) demonstrate that both the rhodochrosite (ranging between 0.06 and 11.31 mol. %; Tab. 5) and the siderite endmembers (ranging between 1.05 and 8.31 mol. %, Tab. 5) are always present in calcite (Fig. 25). Magnesite (lying in the range between 0.57 and 1.79 mol. %; Tab. 5) has nearly no significance in the solid solution.

Strontium, not occurring in the other carbonates, is a characteristic constituent of calcite (especially of type I). The strontianite endmember reaches up to 2.03 mol. % (Tab. 1, column VI). This observation is confirmed by whole-rock compositions of magnetite-rich rocks (Tab. 10) showing that the Sr concentration (in ppm) increases with increasing CaO concentration (in wt. %; Fig. 26). In the presence of relatively high CO_2 concentrations of volcanogenic origin, Ca precipitated directly from the seawater. This origin is confirmed by the observed elevated Sr-concentrations. Fe and Mn are also precipition products from the seawater, but these elements were supplied to the marine basin by volcanogenic activity.

Siderite presented in Fig. 18 ($MnCO_3 – FeCO_3 – CaCO_3$ diagram), shows a wide compositional range varying between 48.48 and 94.57 mol. % $FeCO_3$. Among the other constituents of the solid solution the magnesite endmember (ranging between 0.77 and 24.86 mol. %; Tab. 6) and that of rhodochrosite (0.07 and 35.69 mol. %; Tab. 6) are mostly relatively high, in contrast to calcite which ranges from 0.15 and 18.40 mol. % (Tab. 6).

Rhodochrosite has concentrations of ($FeCO_3 + MnCO_3$) mainly higher than 95 mol. %. Therefore those of calcite and magnesite are relatively low ($CaCO_3$: typically 1.60 – 3.36 mol. %, $MgCO_3$: 0.24 - 2.83 mol. %). The observed compositional variations are caused by zonation. In such a zoned crystal the following chemical variations were detected: a brighter zone of the crystal (in BSE) has the following variations of the endmember concentrations: $MnCO_3$: 78.0 – 92.3; $FeCO_3$: 5.0 – 20.4; $MgCO_3$: 0.7 – 1.8; $CaCO_3$: 0.9 – 3.5 (data in mol. %). In a darker part of the crystal the following endmember concentrations occur: $MnCO_3$: 33.3 – 36.7; $FeCO_3$: 48.5 – 49.3; $MgCO_3$: 13.3; $CaCO_3$: 2.5 – 4.1 (data in mol. %). The darker zone is therefore rhodochrosite-rich siderite, whereas the brighter zone is composed of siderite-rich rhodochrosite. Similar phenomena were also observed in isolated zoned aggregates of Fe–Mn carbonates that are hosted by an odinite matrix from the site "L". For example in sample "L-l" in the cores 81 to 83 mol. % $FeCO_3$ and 10 to 11 mol. % $MnCO_3$ and in the rims 25 to 72 mol. % $FeCO_3$ and 14 to 72 mol. % $MnCO_3$ were analyzed.

The composition of rhodochrosite is presented in Fig. 18 ($MnCO_3 – FeCO_3 – CaCO_3$ diagram). Apart from one exception, the plots show relatively high $FeCO_3$ (up to 21.83 mol. %; Tab. 7) and low $CaCO_3$ (0.52 – 3.36 mol. %; Tab. 7) and $MgCO_3$ concentrations (0.20 – 2.83 mol. %; Tab. 7).

Dolomite and ankerite: Whereas dolomites are relatively pure [$CaMg(CO_3)_2$ ranges from 93.54 – 95.36 mol. %] containing only 3.16 and 3.64 mol. % $CaFe(CO_3)_2$ and excess of $MgCO_3$ (0.82 and 3.30 mol. %), ankerite [$CaFe(CO_3)_2$ ranges from 43.96 to 48.18 mol. %] contains high concentrations of dolomite (36.50 and 37.56 mol. %) and kutnohorite (13.62 and 15.62 mol. %). The chemistry of

dolomite and ankerite is presented in Fig. 18 ($MnCO_3$ – $FeCO_3$ – $CaCO_3$ diagram) showing the composition of dolomite (arrowed from the right side and lying close to the $CaCO_3$-endmember) and ankerite (arrowed from the left side).

Magnetite

Magnetite is mainly associated with siderite and occurs in various shapes. The following magnetite-types were observed:

1. euhedral crystals which may partly show irregular grain-boundaries (Fig. 12 and 15);

2. rare hypidiomorphic to xenomorphic crystals and porous aggregates

3. small lensoidal crystals similar to a rice-grain. Rice-grained magnetite may be concentrated in polycrystalline aggregates (Fig. 11).

4. rounded or globular aggregates and irregular ribbon-like forms with tabular crystals. The latter are of minor abundance.

Magnetite crystals (in particular the rice-grain shaped) are unambiguously pseudomorphic replacements after primary siderite of diagenetic origin (identical to siderite in Phanerozoic ironstones; e. g. Mücke, 2006) according to the equation: $6\ FeCO_3 + O_2 \rightarrow 2\ Fe^{2+}Fe^{3+}_2O_4 + 6\ CO_2$. As a sign of their origin from siderite, the magnetite porphyroblasts of Fig. 12 contain tiny and corroded siderite inclusions representing undigested material. This shows that the above-mentioned reaction was incomplete due to the low-grade metamorphic conditions (see section 8.8). An origin of magnetite from Fe-rich fluids linked with basic volcanites may also be expected.

Sulphides

Two sulphides, detected in this study, are new minerals for the Horní Benešov area.

Cobaltite with the ideal formula CoAsS contains high concentration of Fe and Ni and has the formula of $(Co_{0.63 - 0.76}Ni_{0.12 - 0.21}Fe_{0.15 - 0.20})_{\Sigma=0.90 - 1.17}As_{0.89 - 0.98}S_{0.99 - 1.11}$ (Tab. 9, columns I – III). The mineral composition mentioned under column IV belongs to the linneite group and has the calculated and idealized formula of $Cu_{1.0}(Fe_{1.2}Co_{0.70}Ni_{0.1})_{2.0}(S_{3.5}As_{0.5})_{4.0}$. Such a composition, rich in Fe and Cu, is unknown. Cu-bearing members are known as carrolite $Cu(Co,Ni)_2S_4$ or fletcherite $Cu(Ni,Co)_2S_4$ and Fe-bearing as greigite $FeFe_2S_4$ or violarite $FeNi_2S_4$ (Strunz and Nickel, 2001). According to our knowledge, As-members are completely unknown.

Cobaltite and related minerals (aresenopyrite and mineral of the linneite-group) are probably older than the other sulphides. This is e. g. indicated by the intergrowths between pyrite and arsenopyrite of Fig. 13, where tiny arsenopyrite crystals are intergrown in the same arrangement and size with both, the silicate groundmass and the younger pyrite idioblasts.

The Ni/Co ratio of pyrite is close to 7.2 and thus very similar to that of magnetite, although the correlation of both elements in pyrites is weaker ($R^2 \sim 0.5$) than in magnetites ($R^2 \sim 0.8$). In the plot of Bajwah et al. (1987), the Co/Ni data are lying in the field of "submarine-hydrothermal sedimentary" and „biogenic-sedimentary" pyrite.

Sources of C, O, and S

The fluid $\delta^{18}O$ values calculated from magnetite $\delta^{18}O$ data and bulk range of homogenization temperatures found for iron ores (80-200 °C) vary between +9.0 and +19.0 ‰ SMOW. Similar range in fluid $\delta^{18}O$ values (+8.3 to +11.3 ‰ SMOW) is obtained also for siderite samples and fluid inclusion homogenization temperatures in the respective samples (116-152 °C). Such highly positive fluid $\delta^{18}O$ values are compatible with metamorphic and/or diagenetic waters (Sheppard 1986). This interpretation will not be affected even in case of higher formation temperature (the vitrinite reflectance data are compatible with metamorphic thermal maximum of 200-250 °C, Müller 1981). By contrast, a calcite crystal from drusy vug (sample J.R.) yielded for temperatures 50-61 °C negative fluid $\delta^{18}O$ values (-3.0 to -4.7 ‰ SMOW) suggesting the predominance of meteoric water in the fluid phase.

The fluid $\delta^{13}C$ (H_2CO_3) values of siderite samples calculated for homogenization temperatures found in appropriate samples (116-152 °C) are between -8.3 and -16.3 ‰ PDB. Similar values (-14.7 to -15.2 ‰ PDB) are also obtained for calcite crystals from a vug, HCO_3^- as main career of carbon, and temperatures of 50-61 °C. Such fluid $\delta^{13}C$ values are compatible with mixed nature of carbon dissolved in the fluid phase. The probable sources could include carbon of the host limestones ($\delta^{13}C$ =

~0 ‰ PDB), "deep" carbon (derived from mantle, lower crust, or igneous rocks) or carbon of the homogenized Earth´s crust (averaged from various sources during fluid migration -all the aforementioned sources have $\delta^{13}C$ values between -5 and -8 ‰ PDB), and carbon derived from oxidation of organic matter ($\delta^{13}C$ = -20 ‰ PDB or lower; Hoefs 1997).

The $\delta^{34}S$ values of pyrite from weakly metamorphosed (≤250 °C) iron ores are believed to represent the original pre-metamorphic signature (cf. Hladíková et al. 1990). This is confirmed also by different isotopic composition of pyrites from different lithologies (i.e., iron ores vs. basic volcanites (Fig. 24). The $\delta^{34}S$ values of most pyrite samples from iron ores are highly positive (+16 to +20 ‰ CDT) and coincide with sulphur isotope composition of primary (syn-ore) barite from the polymetallic stratiform deposit at Horní Benešov (+16 to +21 ‰ CDT; Hladíková et al. 1990, Fojt et al. 2010). This implies that the source of sulphur can be the same for both mineralizations. The source of sulphur with the given isotopic composition is invariably interpreted to be in the Devonian marine sulphate (Hladíková et al. 1990, Fojt et al. 2010). In case of pyrite mineralization in iron ores, the reduction of sulphate must take place prior pyrite precipitation. Although the exact mechanism of such reduction remains unclear (bacterial in a closed system, inorganic, or by organic matter), it is evident that virtually all original sulphate must have been reduced to H_2S in order to attain the identical $\delta^{34}S$ value of newly produced sulphide. The rare lighter pyrite $\delta^{34}S$ values could indicate either incomplete reduction of original sulphate, and/or some variations of physico-chemical parameters (Eh, pH) of the fluid during subsequent pyrite precipitation. Pyrites from younger veins having the identical $\delta^{34}S$ values as pyrite in host iron ores originated probably by remobilization of sulphur from host iron ores.

Fluid systems in iron ores

The fluid inclusion and oxygen isotope study suggests the participation of at least three types of fluids during the evolution of the iron ores near Horní Benešov:

1) All samples of iron ores and some samples of crosscutting veins contain an exclusively aqueous fluid phase with low bulk salinity (1-5 wt. % NaCl eq.). The eutectic temperatures indicate the Na-Mg-Cl salt composition. The fluid $\delta^{18}O$ values are highly positive. This fluid endmember most probably represents the fluid phase, which mediated the diagenetic and/or metamorphic recrystallization of rock matrix in this area. In agreement with such interpretation would be also variable homogenization temperatures and subhorizonal distribution of the data in the Th-Tm plot (Fig. 30) which might reflect changing fluid temperature, pressure, or both. Similar metamorphic low-salinity aqueous fluids are described also from polymetallic Zn-Pb deposits near Horní Benešov (Dobeš & Mixa 1993, Fojt et al. 2010) and Horní Město (Fojt et al. 2007).

2) Fluid inclusions from a part of vein- and rock-forming minerals contain high-salinity (up to 24.5 wt. % NaCl eq.) aqueous solution, whose eutectic temperatures (-48 to -56 °C) indicate Na-Ca-Cl composition. Typically these fluids postdate the above mentioned "metamorphic" fluids (the high-salinity fluid inclusions can be considered to be secondary, or they occur in late veins and late fillings of vugs in iron ore samples). Nevertheless in one case (sample BL-63) these fluids represent an episode embedded into the activity of typical metamorphic fluids (Tab. 13). Similar situation has been also observed in stratiform barite at the polymetallic deposit near Horní Benešov, where the syn-metamorphic Na-Ca-Cl brines showed different Na/Ca ratios then post-metamorphic ones (Fojt et al. 2010). This approach is difficult to address in case of iron ores since hydrohalite melting was measured only exceptionally (cf. Tab. 13). Nevertheless the existing data from post-metamorphic settings are comparable to the post-Variscan brines that gave rise to many types of vein mineralizations in the eastern part of the Bohemian Massif (e.g. Fojt et al. 2005, 2007, 2010).

3) Fluid inclusions in calcite crystal contain essentially pure water (Tm-ice as high as 0.0 °C) with negative $\delta^{18}O$ value. These fluids most probably represent latest stage of fluid circulation (cf. the lowermost homogenization temperatures) with the predominance of local meteoric water.

Metamorphism

For the investigated area Kříbek (1977) and Müller (1981) inferred that the temperature of metamorphism is lying at 200-250 °C at maximum, which is just at the border between the zeolite and the greenschist facies. These values are also in good agreement with maximum temperatures obtained

from fluid inclusions (up to 218 °C, Tab. 13). These low-temperature conditions are in agreement with the abundance of relics of clastic material (including fossils) which survived the metamorphism. The low-temperature and low-pressure conditions are indicated also by the occurrence of stilpnomelane and especially by textures with diffusively zoned crystals of Fe-Mn carbonates and remnants of undigested material in replacement textures. The calculated temperatures of formation of chamosite, lying on average between 252 and 306 °C (according to Cathelineau 1988) and 266 and 319 °C (according to Jowett 1991) seem to be in general very high to be realistic. It should be noted that chlorite thermometry often does not offer reliable data and as such it was subject of criticism in the past (e.g. Jiang et al. 1994). In agreement with the low-temperature nature of the investigated ores is the presence of berthierine and odinite. These minerals originate together with dioctahedral smectite and chlorite at relatively low temperatures (up to 150 °C) in a neutral environment where the ratio between the content of iron and clay minerals is higher than 0.5 (Moser-Ruck et al. 2010).

The above mentioned findings about the P-T conditions of metamorphic changes of the iron mineralizations are illustrated in the Fig. 27. The range of P-T conditions is essentially identical with those of the sulphide deposit from Horní Benešov (Fojt et al. 2010).

Ooids in Lahn-Dill type deposits

The occurrence of ooids in Devonian Lahn-Dill type deposits is unknown in the relevant literature. However, some authors of the Horní Benešov iron mineralizations mentioned ooids (Kretschmer 1917, 1918, Karrenberg-Metz & Quitzow 1942, Skácel 1960, 1966), obviously mixing-up collomorphic textures with ooidal structures. However, ooids are known to be typical constituents of the world-wide distributed so-called Phanerozoic ironstones (e.g. in the Ordovician Prague basin) where they were formed under conditions (in a shallow marine basin with slightly agitated water; Mücke 2006, 2008) which do not occur in Lahn-Dill type and related deposits.

Conclusion

Horní Benešov is the only location in the Devonian Vrbno group including the Šternberk-Horní Benešov Belt, where the iron ores occur in immediate association with stratiform sulphide bodies of the VMS/SHMS type.

The Mid-European iron ores of the Devonian Lahn-Dill type represent examples of iron accumulation in a rift setting that are associated with basaltic volcanism (Quade 1976, Sawkins 1990). The emplacement of volcanic rocks later transformed into metavolcanics associated with rift zones was confirmed for the Devonian Vrbno group and the Šternberk-Horní Benešov Belt e.g. by Přichystal (1990) and Kalvoda et al. (2008). For the Lahn-Dill type *sensu stricto*, the basaltic volcanites are considered to be the sources of the iron deposits. These volcanites were transformed during hydrothermal activity into spilites under the release of Fe which was concentrated in the ore body (e. g. Henschel 1960, Flick & Benisch 1990; Nesbor et al. 1993). The spilitized volcanic rocks are well-known from the relevant literature in area of Horní Benešov (Kretschmer 1917, Karrenberg-Metz & Quitzow 1942, Skácel 1960, Barth 1960, Přichystal 1983, 1990), however, they were never observed in a direct contact with iron-rich ore bodies in the Horní Benešov sulphide ore deposit.

As indicated by isotope data, additional sources of ore-forming components in the Horní Benešov deposit were the seawater and sedimentary rocks. According to written communication by J. Hladil (Academy of Science, Prague), the Eifelian-Givetian silty-clayey limestone with carbonate contents up to 80 % and well-preserved fossils was probably a suitable protolith. Under a weak burial, at least a part of the iron ores was formed by ascending Fe-enriched fluids from this protolith.

Therefore, we suggest that the origin of iron ores was a complex process. The studied ore assemblage cannot be considered to be a typical Lahn-Dill ore type *sensu stricto*. Last but not least, there is also a possibility that the given mineralization represents a distal part of the VMS/SHMS mineralization according to the model of Plimer (1979), and, therefore, that it belongs genetically to the suphidic ore deposit. Two types of iron ores were mentioned

already by Reif & Fojt (2001) in the vicinity of Horní Benešov. The hypothesis is supported by the widely accepted opinion that there is a genetic relationship between the sulphide Fe-Zn-Pb±Cu and the oxide-silicate iron-ore mineralizations of stratiform deposits in the Jeseníky Mts (e.g. Havelka 1992).

Many researchers suggest that the Fe-ore deposits of the Lahn-Dill type are relatively older than the VMS/SHMS sulphide deposits in the Jeseníky area (e.g. Skácel 1970; Pouba 1971). In the case of Horní Benešov, where the sulphide and Fe-oxide/silicate ores occur in direct contact, a reversal relationship is observed: the bodies of Fe-ores are present in the hanging-wall of sulphide ores. In one case a small lenticular body of limestone with sulphide mineralization was enclosed in a massive Fe-mineralization. This observation also supports the aforementioned hypothesis of Plimer (1979).

References

Anders E. & Grevesse N. (1989): Abundance of the elements: meteoric and solar. – Geochim. Cosmochim. Acta 53: 197-214.

Babčan J. (1958): Chemicko-mineralogické studium jesenických železných rud. MS, ÚNS Kutná Hora.

Bajwah Z.U., Secombe P.K. & Offler R. (1987): Trace element distribution, Co:Ni ratios and genesis of the Big Cadia iron copper deposit, New South Wales – Australia – Mineral. – Deposita 22: 292-300.

Barth V. (1960): Devonský vulkanismus Šternbersko-hornobenešovského pásma v Nízkém Jeseníku. – Acta Univ. Palack. Olomuc., Fac. rer. Nat. 1, Geol. geogr. biol. 1: 5-131.

Bodnar R.J. (1993): Revised equation and table for determining the freezing point depression of H_2O-NaCl solutions. – Geochim. Cosmochim. Acta 57: 683-684.

Cathelineau M. (1988): Cation site occupancy in chlorites and illites as a function of temperature. – Clay Miner. 23: 471-485.

Chlupáč I. (1965): Fortschritte in der Stratigraphie des Mährischen (Ostsudetischen) Devons. – Geol. Rdsch. 54: 1003-1025.

Clayton R.N. & Mayeda T.K. (1963): The use of bromine pentafluoride in the extraction of oxygen from oxides and silicates for isotopic analysis. – Geochim. Cosmochim. Acta 27: 43-52.

Dobeš P. & Mixa P. (1993): A preliminary fluid inclusion study of the Pb-Zn deposit Horní Benešov, Czech Republic. – Final Meeting of IGCP Project No. 291, Metamorphic fluids and mineral deposits. Abstracts, pp. 17-18. Prague.

Dvořák J., Friáková O., Kukal Z., Otava J. & Přichystal A. (1984): Závěrečná zpráva o komplexním výzkumu vrtu HB SV-3 (Horní Benešov). – ms., Ústř. úst. geol. Praha.

Flick H. & Behnisch R. (1990): Iron ore of the Lahn-Dill type formed by diagenetic seeping of pyroclastic sequences – a case study of the Schalstein section at Gänsberg (Weilburg). – Geol. Rdsch. 79: 401-415.

Fojt B., Dolníček Z., Kopa D., Sulovský P. & Škoda R. (2005): Paragenetická charakteristika hypogenních minerálních asociací uranového ložiska Zálesí u Javorníku ve Slezsku. – Čas. Slez. Muz. Opava (A) 54: 223-280.

Fojt B., Dolníček Z., Hoffman V., Škoda R., Trdlička Z. & Zeman J. (2007): Paragenetická charakteristika ložisek Zn-Pb rud v širším okolí Horního Města u Rýmařova (Nízký Jeseník). – Acta Mus. Moraviae, Sci. geol. 92: 3-57.

Fojt B., Dolníček Z., Hladíková J., Škoda R. & Zeman J. (2010): Paragenetická charakteristika ložisek Zn-Pb a Fe rud u Horního Benešova v Nízkémm Jeseníku. – Část I.: Ložisko Zn-Pb rud. – Čas. Slez. Muz. Opava (A) 59: 1-59.

Franke W. & Żelaźniewicz A. (2000): The eastern termination of the Variscides: terrane correlation and kinematic evolution. In: Franke W., Haak V, Oncken O., Tanner D. (eds). Orogenic Processes: Quantification and Modelling in Variscan Belt. – Geological Society London Speciál Publications 179: 63-86.

Grygar R. & Vavro M. (1995): Evolution of Lugosilesian Orocline (north-eastern perifery of the Bohemian Massif): Kinetice of Variscan deformation. – J. Czech. Geol. Soc. 40: 65-90.

Havelka J. (1992): General genetic model and roots of flow metal contents of the Jeseníky Mts. Deposits of stratiform sulphide formation. – Sbor. věd. prací VŠB v Ostravě, ř. horn.-geol. 38: 89-101.

Hentschel H. (1960): Zur Frage der Bildung der Eisenerze vom Lahn-Dill Typ. – Freib. Forschungsh. 79: 82-105.

Hladil J., Kalvoda J. & Vavrdová M. (1987): Některá nová mikropaleontologická data z Nízkého Jeseníku. – Zem. plyn nafta, 6: 97-118.

Hladíková J., Šmejkal V., Fojt B., Pertold Z. & Aichler J. (1990): Izotopické složení síry, uhlíku a kyslíku vybraných lokalit Jeseníků. – Sbor. geol. věd, ř. lož. geol. mineral. 29: 141-165.

Hoefs J. (1997): Stable isotope geochemistry, 4th ed., Springer Verlag, Berlin, New York.

Hornibrook R. C. & Longstaffe (1996): Berthierine from the Lower Cretaceous Cölearwater Formation, Alberta, Canada. – Clay and Clay minerals 44: 1-21.

Houzar S., Cempírek J., Fojt B., Gadas P., Hrazdil V., Novák M., Sejkora J. & Škoda R. (2010): Přehled nových minerálů nalezených na Moravě a ve Slezsku v letech 1985-2009. – Acta Mus. Moraviae, Sci. geol. 95: 5-60.

Jakeš P. & Patočka F. (1982): Compositional variations of the Devonian volcanic rock sof the Jeseníky Mts. – Věst. Ústř. Úst. Geol. 57: 139-202.

Janečka J. & Skácel J. (1950): Zpráva o geologickém mapování v oblasti Horního Benešova. – Přír. Sbor. Ostrav. kraje 11: 162-173.

Jiang W.-T., Peacor D.R. & Buseck P.R. (1994): Chlorite geothermometry? – Contamination and apparent octahedral vacancies. – Clays Clay Miner. 42: 593-605.

Jowett E.C. (1991): Fitting iron and magnesium into the hydrothermal chlorite geothermometer. GAC/MAC/SEG Joint Annual Meeting, Toronto. Program with abstracts 16: A62.

Kalvoda J., Bábek O., Fatka O, Leichmann J., Melichar R., Nehyba S. & Špaček P. (2008): Brunovistulian terrane (Bohemian Massif Central Europe) from late Proterozoic to late Paleozoic: a review. – Int. J. Earth Sci. (Geol. Rdsch.) 97: 497-518.

Karrenberg-Metz H. & Quitzow H.W. (1942): Die Erze des schlesisch-mährischen Devons. – Arch. Lagerst. Forschung 75: 155-166.

Kettner R. (1952): Zpráva o mapování v okolí Horního Benešova a Leskovce. – Věst. Ústř. Úst. Geol. 27: 149-155.

Kopecká L. (2012): Mineralogie rud typu Lahn-Dill ve šternbersko-hornobenešovském pruhu. – ms., Diploma thesis, PřF UP Olomouc.

Koutek J. (1951): K petrografii železnorudných ložisek v nemetamorfovaném devonu moravsko-slezských Jeseníků. – Věst. Ústř. Úst. Geol. 22: 55-58.

Kretschmer F. (1917): Die erzführende Diabas- und Schalsteinzone Sternberg-Benisch. – Arch. Lagerst. Forschh. 23: 1-198.

– (1918): Über die Eisensilikaterze des Diabas- und Schalsteinzuges Sternberg-Benisch. – N. Jb. Min., Geol., Pal. (1918): 19-42.

Kruťa T. (1958): Mineralogické poměry na ložisku barevných kovů, železných rud a barytu v Horním Benešově ve Slezsku. – Acta Mus. Moraviae, Sci. nat. 46: 5-38.

Kříbek B. (1977): Uhlíkaté formace Českého masivu a jejich mineralizace. – Knih. Čes. Geol. Úst. 66: 1-126.

Kuba B. & Urbánek J. (1978): Nové poznatky z ložiska Pb – Zn rud v Horním Benešově. – ms., GP Rýmařov.

Kučera J. (1957): Závěrečná zpráva a výpočet zásob na Fe-ložisku Horní Benešov. – ms., Geofond Praha.

McLennan S.M. (1989): Rare earth elements in sedimentary rocks: Influence of provenance and sedimentary processes. – Rev. Mineral. 21: 169-200.

Melka K. & Vybíral J. (1977): Geologická stavba ložisek železných rud v Hornomoravském úvalu a jejich Fe-fylosilikátů. – Sbor. geol. věd, lož. geol. mineral. 18: 32-88.

Mosser-Ruck R., Cathelineau M., Guillaume D., Charpentier D., Rousset D., Barres O. & Michau N. (2010): Effects of temperature, pH, and iron clay and liquid/clay ratios on experimental conversion on dioctahedral smectite to berthierine, chlorite, vermiculite, or saponite. – Clay Clay Mineral. 58: 280-291.

Mücke A. (2006): Chamosite, siderite and the environmental conditions of their formation in chamosite-type Phanerozoic ooidal ironstones. – Ore Geol. Rev. 28: 235-249.

– (2008): Ooide und Sphärolithe: Genese und Unterscheidungsmerkmale zweier rundlicher Gebilde, die in der Natur weit verbreitet sind. – Aufschluss 59: 181-191.

Mücke A., Fojt B. & Dolníček Z. (2010): Petrography, mineralogy, geochemistry and genetic aspects of the Lahn-Dill type deposit of Malý Děd (= Leiterberg) in Devonian Vrbno Group (Silesicum), Czech Republic. – Acta Mus. Moravice, Sci. geol. 95: 95-129.

Müller P. (1981): Reflektivita organických dispersinitů ve vzorcích vrtu HB-SV-1. – In: Dvořák J. (ed.): Vrt Horní Benešov HB-SV-1. MS, ČGÚ Praha.

Nesbor H.D., Buggisch W., Flick H., Horn M. & Lippert H.J. (1993): Vulkanismus im Devon des Rhenohercynikums. Fazielle und paläogeographische Entwicklung vulkanisch geprägter mariner Becken am Beispiel des Lahn-Dill Gebietes. – Geol. Abh. Hessen 98: 3-87.

Newberry N.G., Peacor D.R., Essene E.J. & Geissman J.W.(1982): Silicon in magnetite: High resolution microanalysis of magnetite-ilmenite intergrowths. – Contrib. Mineral. Petrol. 80: 334-340.

Ohkawa M., Niyagara M., Ohta E. & Hoshiro K. (2007): Silicon substituted magnetite and accompanying iron oxides and hydroxides from the Kumano mine, Yamaguchi Prefecture, Japan: Reexamination of the so-called maghemite (γ-Fe$_2$O$_3$). – J. Mineral. Petrolog. Sci. 102: 182-193.

O'Neil J.R., Clayton R.N. & Mayeda T.K. (1969): Oxygen isotope fractionation in divalent metal carbonates. – J. Chem. Phys. 51: 5547–5558.

Orel P. (1975): Variský tektonický styl paleozoika západní části jesenického bloku Českého masivu. – Výzk. pr. Ústř. Úst. Geol. (1975): 5-23.

Plimer I.R. (1979): Sulphide rock zonation and hydrothermal alteration at Broken Hill, Australia. – Trans. Inst. Min. Metall. (Sect. B: Appl Earth Sci) 88: 161-176.

Pouba Z. (1971): Vztahy mezi petrogenezí a mineragenezí ultrabazických a bazických magmatitů Hrubého Jeseníku. – In: Mísař Z. (ed.): Ultrabasity a ultramafity, ÚGV UK, Praha, pp. 196-203.

Pouchou J. & Pichoir F. (1985): „PAP" procedure for improved quantitative microanalysis. – Microbeam Anal. 20: 104-105.

Přichystal A. (1983): Vulkanické horniny ze strukturního vrtu HB SV 1. – Sbor. ref. semináře Geofyz. Brno: (1983). 69-73.

– (1984): Geologie a petrologie šternbersko-chabičovské vulkanické struktury nízkém Jeseníku. – Sbor. „Nové poznatky o geologii Jeseníků": (1984): 45-46.

– (1990): Hlavní výsledky studia paleozoického vulkanismu ve šternbersko-hornobenešovském pruhu (Nízký Jeseník). – Sbor. geol. věd, Lož. geol. mineral. 24: 41-66.

Reif J. (1985): Mineralogie železorudných výskytů na ložisku Pb-Zn rud v Horním Benešově. – MS, Diploma thesis PřF MU Brno.

– (1999): Výskyt karbonátových Mn rud na stratiformním sulfidickém ložisku Horní Benešov. – Seminář „Současné výzkumy v sileziku", PřF MU, Brno, pp. 33-38.

– (2000a): Mineralogie železných rud na ložisku Pb-Zn-Ag a barytu v Horním Benešově. – ms., doktorská disertace PřF MU Brno.

– (2000b): Occurrence of manganese carbonate ores on strata-bound Horní Benešov deposite (Silesia, Czech Republic). – Věst. Čes. geol. úst. 75: 449-453.

Reif J. & Fojt B. (2001): Mineralogy and geochemistry of iron ores from Horní Benešov deposit. – Mitt. Österr. Miner. Ges. 146: 254-255.

Reif J. & Vávra V. (2000): Scheelit z železných rud na ložisku Zn, Pb, Ag a barytu v Horním Benešově (preliminary information). – Geol. výzk. Mor. Slez. v r. 1999. Brno.

Reynolds J. & Goldstein R. (1990): Systematics of fluid inclusions in authigenic minerals and applications in a sedimentary basin analysis. Short course at the University of Manchester, 83 pp.

Roemer F. (1870): Geologie von Oberschlesien. Breslau.

Quade H. (1976): Genetic problems and environmental features of volcano-sedimentary iron ore deposits of the Lahn-Dill type. – In: Wolfe K.H. (ed): Handbook of strata- bound and stratiform ore deposits. Elsevier Amsterdam, pp. 255-294.

Sawkins F.J. (1990): Metal deposits in relation to plate tectonics, second edition. Springer Verlag. Berlin Heidelberg, New York.

Sawkins F.J. & Burke K. (1980): Extensional tectonics and Mid-Paleozoic massive sulphide occurrences in Europe. – Geol. Rdsch. 69: 349-360.

Schulmann K. & Gayer R. (2000): A model for a continental accretionary wedge by oblique collision. – J. Geol. Soc. 157: 401-416.

Sheppard S.M.F. (1986): Characterization and isotopic variations in natural waters. – Rev. Mineral. 16: 165-183.

Skácel J.(1959): Železnorudná ložiska Jeseníků. – Geol. průzk. 11: 334-337.

– (1960): Geologie devonu a rudních ložisek u Horního Benešova. – Přír. čas. slezský 21: 465-488.

– (1962): Metallogenetische Verhältnisse der Mittel- und Ostsudeten (ČSSR) – Zeitschr. Angew. Geol. 9: 469-475.

– (1963a): Úlomkovité železné rudy na ložiskách ve východosudetském devonu. – Zprávy Slez. úst. ČSAV v Opavě, přír. vědy 126: 1-4.

– (1963b): Železorudná ložiska typu „Lahn-Dill" v durynském devonu a jejich přirovnání k našim. – Geol. průzk. 5: 3-4.

– (1964): Die Eisenerzlagerstätten des mährisch-schlesischen Devons. – Ber. Geol. Ges. DDR 9: 487-506.

– (1965): Oolitické železné rudy v moravskoslezském devonu a problém geneze ložisek typu Lahn-Dill. – Čas. Slez. Muz. Opava (A) 14: 111-114.

– (1966): Železorudná ložiska moravskoslezského devonu. – Rozpr. ČSAV, ř. mat. přír. věd 76: 3-60.

– (1970): Poznámky ke vztahu devonských Fe-ložisek ke kyzovým ložiskům s polymetaly na sv. okraji Českého masívu. – Acta Univ. Palack. Olomuc., Fac. rer. nat. 29: 149-157.

Slack J.F., Jiang W.-T., Peacor D.R. & Okita, P.M. (1992): Hydrothermal and metamorphic berthierine from the Kidd Creek volcanogenic massive sulphide deposit, Timmins, Ontario. – Can. Min. 30: 1127-1142.

Strunz H. & Nickel E.H. (2001): Mineralogical Tables. Schweizerbart'sche Verlagsbuchhandlung. Stuttgart.

Synek J., Rajlich P. & Urban M. (1990): Transpression and transtension in the Devonian and Culm of the Nízký Jeseník Mts. – Acta Univ. Carol., Geol. 2: 209-234.

Urbánek J. (1988): Poznatky z revizního průzkumu ložiska Horní Benešov. – Geol. průzk. 30: 193-197.

Wedepohl K.H. (1975): Handbook of Geochemistry. Springer-Verl. Stuttgart.

Zachař Z. (1983): Mineralogie chloritů železorudných výskytů ve šternbersko-hornobenešovskémk pruhu. ms., diploma thesis, PřF UJEP Brno.

Zelinger O. (ed.) (1998): RD Jeseník. Jeseník.

Zheng Y.-F. & Simon K. (1991): Oxygen isotope fractionation in hematite and magnetite: A theoretical calculation and application to geothermometry of metamorphic iron-formation. – Eur. J. Mineral. 3: 877-886.

Zimák J. (1999): Stilpnomelan z akumulací Fe-rud lahn-dillského typu ve šternbersko-hornobenešovském pruhu a vrbenské skupině. Seminář „Současné výzkumy v Sileziku", Brno, pp. 29-32.

– (2004): Fylosilikáty ložisek typu Lahn-Dill na území Moravy a Slezska. – Sbor. Mineralógia Západných Karpát a Českého masivu (2004): 72-75.

Zimák J. & Vávra V. (1998): Monazit v silikátových Fe-rudách typu Lahn-Dill u Chabičova. – Geol. výzk. Mor. Slez. v r. 1997 5: 72-73.

Zimák J., Vávra V. & Krausová D. (1998): Výskyt barytu ve stilpnomelanové Fe-rudě z důlní míry Prokop u Šternberka. – Geol. výzk. Mor. Slez. v r. 1997 5: 75-76.

Authors' addresses: Arno Mücke, Experimentelle und Angewandte Mineralogie, Göttinger Zentrum Geowissenschaften, Georg-August-Universität, Goldschmidtstrasse 1, 37077 Göttingen, Germany. E-mail: arhemucke@gmx.de (Corresponding author)

Zdeněk Dolníček, Department of Geology, Palacký University, Tř. 17, listopadu 12, 771 46 Olomouc, Czech Republic. E-mail: dolnicek@prfnw.upol.cz

Bohuslav Fojt, Jaroslav Reif & Radek Škoda, Institute of Geological Sciences, Masaryk University, Kotlářská 2, 611 37 Brno, Czech Republic.
E-mail: fojt@sci.muni.cz

Jana Hladíková, Czech Geological Survey, Geologická 6, 152 00 Prague, Czech Republic. E-mail: jhladikova@twobears.cz

Marta Pudilová, Faculty of Sciences, Charles University, Albertov 6, 128 43 Prague, Czech Republic. E-mail: pudilova@natur.cuni.cz